International Journal of Biological Macromolecules 309 (2025) 142843

Contents lists available at ScienceDirect

International Journal of Biological Macromolecules

journal homepage: www.elsevier.com/locate/ijbiomac

A first-in-class non-cytotoxic nanocarrier based on a recombinant human ferritin boosts targeted therapy, chemotherapy and immunotherapy

Giada Tisci [a,1], Lenka Rajsiglova [b,c,1], Sandra Bibbo [d,e], Giovanna Zicchedduf [f], Elena Ricciardi [f], Elisabetta Falvo [g], Vincenzo De Laurenzi [d,e], Gianluca Sala [d,e,*], Emily Capone [d,e], Gianni Colotti [g], Alessandro Arcovito [h,i], Noah Giacon [h], Peter Makovický [j], Leonid Sushytskyi [b,k], Pavol Lukac [b,c], Luca Vannucci [b], Patrizio Giacomini [l], Pierpaolo Ceci [g,m,**]

[a] Department of Biochemical Sciences, Sapienza University, Rome, Italy
[b] Laboratory of Immunotherapy, Institute of Microbiology, Czech Academy of Sciences, Prague, Czech Republic
[c] Department of Cell Biology, Faculty of Science, Charles University, Prague, Czech Republic
[d] Department of Innovative Technologies in Medicine & Dentistry, University of Chieti-Pescara, Chieti, Italy
[e] Center for Advanced Studies and Technology (CAST), Italy
[f] Translational Oncology Unit, IRCCS National Cancer Institute Regina Elena, Via Elio Chianesi 53, Rome, Italy
[g] Institute of Molecular Biology and Pathology, Italian National Research Council IBPM-CNR, Rome, Italy
[h] Dipartimento di Scienze Biotecnologiche di Base, Cliniche Intensivologiche e Perioperatorie, Università Cattolica del Sacro Cuore, Largo F. Vito 1, Rome, Italy
[i] Fondazione Policlinico Universitario "A. Gemelli", IRCCS, Largo Agostino Gemelli 8, 00168 Rome, Italy
[j] Institute of Histology and Embryology, Faculty of Medicine, University of Ostrava, Syllabova 19, Ostrava-Vítkovice, Czech Republic
[k] Department of Carbohydrates and Cereals, Faculty of Food and Biochemical Technology, University of Chemistry and Technology in Prague, Technická 5, 166 28 Prague, Czech Republic
[l] UOSD Medicina di Precisione in Senologia, Fondazione Policlinico Universitario "A. Gemelli", IRCCS, Largo Agostino Gemelli 8, Rome, Italy
[m] Thena Biotech, Latina, Italy

ARTICLE INFO

Keywords:
Human ferritin nanocarrier
Peptide grafting
cancer therapy booster

ABSTRACT

To address the challenge of drug accumulation and penetration at the tumor site(s), herein we describe a first-in-class nanocarrier containing 24 copies each of two bioactive peptides (BAPs) genetically fused in frame to the 24 N-termini of a human ferritin H-type construct, named THE-10. The two BAPs are specific for PD-L1 and integrin αVβ3/αVβ5 plus Neuropilin (iRGD) respectively, conferring immune checkpoint blockade and drug-internalization properties. In turn, the THE-10 backbone brings 48 BAPs contiguous for synergism, prolonged blood half-life, and release into the tumor microenvironment upon conditional cleavage of a metalloprotease-sensitive site. Predicted THE-10 multitasking activity was experimentally supported as follows. Size-exclusion chromatography and surface plasmon resonance demonstrated BAP cleavage/release and receptor binding (nanomolar K_D). Live-cell/time-lapse imaging demonstrated 4-fold-increased internalization of naked therapeutic antibodies, mirrored by enhanced cytotoxicity of the corresponding Antibody-Drug Conjugate. Slight antitumor effects were observed in vivo by treating immune checkpoint-sensitive syngeneic mouse colorectal model with THE-10 alone. Drug boosting was instead considerable on colorectal and pancreatic tumor allografts when THE-10 was co-administered with both small and large chemotherapeutic agents, outperforming the original iRGD cyclic peptide. Thus, THE-10 may enhance target therapy, chemotherapy and immunotherapy altogether, e.g. it candidates as a multitasking, all-round, antineoplastic therapy booster.

* Correspondence to: G. Sala, Department of Innovative Technologies in Medicine & Dentistry, University of Chieti-Pescara, Chieti, Italy.
** Correspondence to: P. Ceci, Institute of Molecular Biology and Pathology, Italian National Research Council IBPM-CNR, Rome, Italy.
E-mail addresses: g.sala@unich.it (G. Sala), pierpaolo.ceci@cnr.it (P. Ceci).
[1] The authors contributed equally to this work.

https://doi.org/10.1016/j.ijbiomac.2025.142843
Received 9 January 2025; Received in revised form 31 March 2025; Accepted 2 April 2025
Available online 3 April 2025

1. Introduction

Cancer ranks as a leading cause of death and an important barrier to increasing life expectancy worldwide [1]. Despite fast-paced drug discovery, survival in advanced cancer remains low [2]. Major challenges of current anticancer regimens are poor drug penetration into the tumor mass, short blood half-life, prominent side effects, and induction of pharmacological resistance [3,4]. Enhancing drug accumulation at the tumor site(s) may address the above limitations altogether, but penetration deep into the tumor microenvironment (TME) is critical.

Among several approaches, bioactive peptides (BAPs) are being developed crossing the TME penetration barrier, enhancing drug delivery, and improving targeting [5–7]. Certepeptide (also known as internalizing RGD, iRGD) is a 9-amino acid cyclic peptide (CRGDKGPDC) that binds the αVβ3 and αVβ5 integrins on the tumor blood vessels through its Arg-Gly-Asp (RGD) motif, enhancing tumor penetration and therapeutic activity of iRGD-conjugated or co-administrated drugs [8–10]. Upon cleavage, the iRGD peptide exposes its C-terminal region, binds the neuropilin-1 (NRP-1) receptors, and consequently triggers NRP-1-dependent endocytosis, further improving tumor drug penetration (C-end rule or CendR) [11].

BAPs may also be applied to mimic immune checkpoint inhibitors (ICI). These therapeutic antibodies effectively relieve the negative impact of an immune-suppressive TME by binding molecules such as the Cytotoxic T-lymphocyte-associated antigen 4 (CTLA4) or programmed cell death protein 1 (PD-1) and its PD-L1 ligand [12], but cost, in vivo immunogenicity and side effects remain major ICI drawbacks [11]. Fortunately, ICI-like BAPs have now been identified by screening phage-display peptide libraries [13]. CLQKTPKQC and CVRARTR (PD-L1Pep-1 and PD-L1Pep-2 respectively) and GNWDYNSQRAQLYNQ, block PD-L1 and PD-1 respectively, and are active both in vitro and in vivo [14,15]. Their major advantages over antibodies are improved tissue penetration, lower immunogenicity, and moderate manufacturing costs.

Thus, short iRGD and ICI-like BAPs candidate for therapeutic application, but some drawbacks remain, including weak binding affinity, low persistence in blood, and susceptibility to degradation [16]. One way they may be effectively mitigated is by introducing multiple BAP copies (for additive effects) into a supramolecular protective structure. Organic and inorganic vehicles such as liposomes, nanopolymers, nanocrystals, nanoshells, and dendrimers may be considered, since they are optimized to carry covalently bound, entrapped, and/or surface-absorbed active biomolecules and anti-cancer drugs. Their advantages include modular construction, ability to incorporate different chemical species, versatility, proven drug delivery properties, derivatized with tumor-targeting moieties, including anti-tumor antibodies [17–20]. However, the formulation of organic and inorganic vehicles often requires challenging multi-step protocols, and may not be easily translated into a highly standardized, Good Manufacturing Process (GMP)-compliant process.

Therefore, when it comes to small polypeptides such as BAPs (e.g. iRGD and PD-L1Pep-1) it may be practical to consider their incorporation, by recombinant DNA approaches, at specific positions into the primary sequence of a selected polypeptide backbone. This may hopefully result in BAP proximity, biological synergy, controllable stoichiometries, and high, defined multiplicities. Moreover, in this approach BAPs may be made conditionally releasable by design. Finally, one-step whole gene synthesis of protein fusions is routinely possible, and technologically appealing.

Yet, not all protein may be suitable. Grafting multiple BAPs onto a recombinant protein requires several unique properties, including a resilient three-dimensional folding tolerant to multiple simultaneous substitutions in different regions, a proven carrier ability, a strong tropism for its target (ideally for multiple tumors), a controlled release of BAPs in a biologically active form and, last but not least, an effective, industrial-grade biomanufacturing pipeline, possibly in low-cost bacterial hosts.

Protein nanocarriers, due to their size and customizable design may be optimal to dispatch BAPs and, among them, H-type human ferritin (HFt) is a good candidate, at least in principle. HFt is a highly symmetrical multimeric protein consisting of 24 subunits. It may be synthesized in bacterial hosts and, under appropriate conditions it spontaneously refolds in a cell-free system. HFt forms an essentially spherical shell enclosing a hollow cavity that physiologically stores iron, but can be adapted to accommodate cytotoxic drugs, effectively delivering them to iron-hungry, actively proliferating cells, which by itself makes HFt tumor-selective. HFt variants have been generated by several groups [21–35], but two unique add-ons have been developed by us to enhance HFt-mediated tumor targeting and introduce conditional TME delivery.

The first add-on is PASylation, e.g. a masking polypeptide sequence rich in proline (P), alanine (A), serine (S) and Glutamic Acid (E) residues (PASE). When genetically fused to the N-terminus of each HFt subunit, PASE improves chemical stability and shelf life, and lowers HFt binding affinity for its cellular ligand, the transferrin receptor (CD71). Then, PASE prevents the massive quick dispatch that is crucial for physiological iron supply, but becomes undesirable when a cytotoxic payload has to be slowly released into the TME. Accordingly, HFt PASylation was shown to increase in vivo half-life, improving drug delivery and therapeutic efficacy [36].

The second add-on is a sequence responsive to proteolytic digestion by tumor metalloproteases (MMPs 2 and 9, hence MP sequence) inserted right below the outer PASE polypeptide. Cleavage at the MP site and release of the shielding moieties may occur only after HFt has reached its intended destination in the TME, conditionally restoring high CD71 binding affinity right in the surroundings of the tumor [36].

Both add-ons were introduced in a previously described, genetically engineered HFt prototype named THE-05 that, when loaded in its hollow cavity with a selected topoisomerase inhibitor, was shown to be curative in several mouse tumor allograft and xenograft models [21,37], and to have a favorable toxicologic profile despite it carries about 75 molecules of a highly toxic payload. A first-in-human phase 1 clinical trial with this THE-05 derivative, called THE-0504 is presently ongoing and actively recruiting.

The many favorable features of the first-in-class THE-05 backbone make it the ideal ‘template’ to be turned into a novel BAP nanocarrier, called THE-10, that is the subject of the present report. THE-10 is empty, e.g. it does not exploit the cargo abilities of HFt, but rather its unique quaternary structure whereby the N-terminal ends of the 24 monomers facing outward, known to be resilient to amino acid substitutions, have been further modified to include multiple MP sites and 24 copies each of two modified linear versions of the selected BAPs, namely the above-mentioned PD-L1 binding peptide (PD-L1Pep-1) and the integrin αVβ3/αVβ5 and NRP-1 binding peptide (iRGD).

Herein, we describe this novel THE-10 construct, providing in vitro and in vivo evidence that it retains the favorable features of parental THE-05. At variance from the purely cytotoxic THE-0504 nanocarrier, THE-10 is not cytotoxic per se, but it boosts the anti-tumor effects of different classes of co-administered drugs, including small molecules and Antibody-Drug Conjugates (ADCs). Additionally, THE-10 exerts ICI-like effects. Given the diversity (biological and conceptual) of these effects, THE-10 testing, reported herein for the first time, was carried out in the very same in vitro and in vivo models selected for the development of the naked parental BAP. Data to be shown demonstrate therapeutic boosting despite the diverse experimental models, and regardless of the biochemical properties, size, and mechanism of action of the co-administered drug.

2. Materials and methods

2.1. Design of the THE-10 nanocarrier

THE-10 is a variant of an HFt-MP-PASE construct (THE-05),

previously described [22,36]. Three THE-10 functional domains may be distinguished (Scheme 1), C- to N-terminus, as follows. Domain 1, encoding the amino acid sequence of the native human ferritin HFt. Domain 2, encoding two amino acid sequences: (i) the PD-L1 binding peptide LQKTPKQ conjugated to the N-terminal of domain 1 through the amino acid sequence PLGLAG, that corresponds to the matrix metalloproteinase (MMP) cleavage site; and (ii) the tumor penetrating peptide amino acid sequence RGDKGPD, conjugated to LQKTPKQ through a second MMP cleavage site. Domain 3 is at the N-terminal extreme, and comprises a proline, serine, alanine and glutamate (PASE) repeat: ASPAAPAPASPAEPAPSAPAASPAAPAPASPAEPAPSAPA.

2.2. Cloning, overexpression and purification of the THE-10 construct

The *THE-10* DNA sequence was codon-optimized for high level expression in *Escherichia coli*, produced by whole-gene synthesis at GENEART AG (Germany), cloned into the expression vectors pET-27b (Thermo Fisher Scientific Waltham, USA), and expressed in the BL21 (DE3) bacterial host (New England BioLabs, Ipswich, USA). *E.coli* cells were grown to an optical density (OD) at 600 nm of 1.0 at 37 °C in 1 L of terrific broth medium (Grisp, Porto, Portugal) containing kanamycin (Serva, Heidelberg, Germany) at a final concentration of 0.03 mg/mL. At this OD, gene expression was induced by the addition of 1 mM isopropyl-1-thio-β-D-galactopyranoside (IPTG), and *E. coli* was incubated overnight at 37 °C. The cells were harvested by centrifugation at 5000 rpm for 20 min at 4 °C. The recovered pellet was suspended in 90 mM Tris-HCl, 50 mM NaCl and EDTA 0.5 mM at pH 9 and incubated at 60 °C for 15 min. After thermal treatment, the enzyme DENARASE (c-LEcta GmbH, Leipzig, Germany) was added at 15 U/mL to cleave DNA and RNA impurities, and then the cells were disrupted by sonication. The lysate was centrifuged at 14,000 rpm for 50 min at 4 °C and the supernatant was further treated at 72 °C for 8–10 min. The solution was centrifuged 14,000 rpm for 50 min at 4 °C. The supernatant was dialyzed overnight against phosphate-buffered saline (PBS) pH 7.5, concentrated by means of 100 kDa Amicon Ultra-15 centrifugal filter devices (Millipore, Billerica, USA) and loaded on a strong basic anion-exchange filter, Sartobind Q (Sartorius, Goettingen, Germany), previously equilibrated with the same buffer. THE-10 preparations were eluted from the column, whereas other *E. coli* impurities were retained by the filter. Finally, the THE-10 samples were sterile-filtered and stored at 4 °C (short-term) or −20 °C (long-term). Typical yields were 100 mg of pure proteins per 1 L of bacteria culture.

Protein stability was assessed both in buffer and in serum. THE-10 samples at 1 mg/mL were incubated for different times (0–18 h) at 37 °C in PBS buffer or serum (OptiClone Serum, Euroclone spa, Milan, Italy). Reactions were stopped by moving the mixture to −20 °C and, after 24 h, by boiling at 99 °C for 5 min in the presence of 10 % SDS. Reaction mixtures were visualized by SDS-PAGE, running the samples side by side with Opti-Protein XL protein markers (Applied Biological Materials Inc. Richmond, BC, V6V 2J5, Canada) on 15 % gels, and staining with Coomassie brilliant blue.

2.3. Protein characterization

The purity of all the preparations was assessed by SDS-PAGE, running the samples on 15 % gels and staining with Coomassie brilliant blue. Opti-Protein XL was used as protein marker in the gel. Protein concentration was determined spectrophotometrically at 280 nm, using a molar extinction coefficient (on a 24-mer basis) of 4.54×10^5 M-1 cm-1 (ProtParam software, http://www.expasy.org). Size-Exclusion Chromatography (SEC) was performed using a Superose 6 Increase 10/300 GL (Cytiva Sweden AB, Uppsala) gel-filtration column equilibrated with PBS at pH 7.4. Superose 6 Increase 10/300 GL is a prepacked column for high-resolution size exclusion chromatography in small-scale (sample volume < 500 μL) preparative purification. It is also suitable for the characterization and analysis of proteins and other biomolecules with molecular weights between 5000 and 5000,000 Da. All the evaluated samples were prepared at 1 mg/mL in filtered PBS. All the traces of SEC experiments were analyzed with QtiPlot (IONDEV SRL, Bucuresti, Romania).

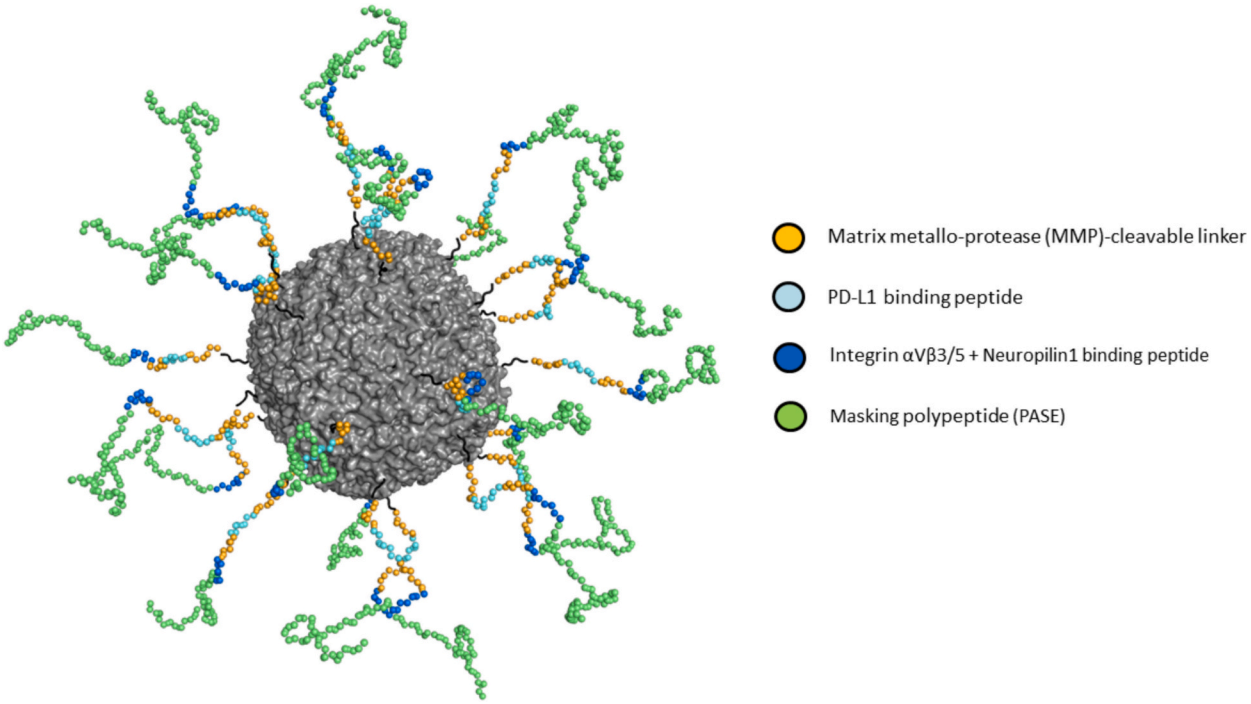

Scheme 1. Three-dimensional view of the THE-10 construct. Prediction and analysis of the protein structure was achieved by using the software Modeller 10.6 (https://salilab.org/modeller/).

2.4. In vitro release of PASE and multiple peptides from THE-10 in the presence of MMP2/9 proteases

To assess the peptides release after enzymatic cleavage, THE-10 cleavage was studied in the presence of the specific proteases MMP-2/9. THE-10 solutions were mixed with collagenase IV (Collagenase Type 4 containing MMP2 and 9, *Clostridium histolyticum*, Pan-biotech, Leipzig, Germany) and incubated at 37 °C for 2 h. Samples were then analyzed by SEC using a Superose 6 gel-filtration column equilibrated with PBS at pH 7.4 in native conditions, or by SDS-PAGE gel chromatography by boiling at 99 °C for 10 min in the presence of 10 % SDS. SDS PAGE was stained with Coomassie brilliant blue R-250.

2.5. Testing of the THE-10 fusion protein binding ability by Surface Plasmon Resonance experiments

Surface Plasmon Resonance (SPR) was carried out to assess the thermodynamic and kinetic parameters of the interaction between the construct THE-10 (analyte) and its specific receptors (ligands): αVβ3, NRP-1 (αVβ3 #IT3-H52E3, his-tagged human #NR1-H5228; ACROBiosystem, Germany), and PD-L1 (C-terminal his-tagged human PD-L1 #10084-H08H, Sino Biological Europe GmbH, Germany) in a Biacore X-100 apparatus. The ligands were immobilized on a Sensor Chip NTA. The NTA group was activated by nickel ions (Ni^{2+}) to bind selectively histidine-tagged ligands. Ligands (αVβ3 or NRP-1: 25 μg/mL and PD-L1: 50 μg/mL) were stripped by sequestering nickel ions with EDTA (regeneration phase). After ligand immobilization, THE-10 was prepared, diluted and injected in sterile HEPES 20 mM, pH 7.4, NaCl 150 mM, 0.005 % surfactant Tween20 (buffer HST) at different concentrations (indicated as 24-mer ferritin molar concentration): αVβ3 and NRP-1: 96, 192, 384 (tested twice to ensure reproducibility of the results), 768 and 1536 nM; PD-L1: 6.25, 12.5, 25, 50, 100 and 200 nM. As a negative control, sensor chips were treated as described above in the absence of immobilized ligand. Full data fitting with models envisaging 1 and 2 interaction sites was computed from overall kinetic evaluation of the sensorgrams using the Biacore X100 evaluation software (2.0.1 plus package).

2.6. Flow cytometry

To assess surface markers, cells were stained with anti-HER2 Trastuzumab (Roche Pharmaceuticals injectable preparations obtained from the hospital pharmacy of the Regina Elena Cancer Institute), or with the following monoclonal antibodies (mAbs): anti-human CD51/CD61 FITC (Integrin αVβ3) Clone: 23C6 (Cat#11-0519-41, eBioscience) and anti-human CD304 PE (Neuropilin-1) Clone: 12C2 (Cat#354503, Biolegend). Cells were stained with anti-CD51/CD61 or anti-CD304 mAbs (1:20) or with anti-HER2 (10 μg/mL) in cold PBS-2 % FBS solution, 30 min on ice, and washed three times. F(ab')2-Goat anti-Human IgG Fc Cross-Adsorbed Secondary Antibody, FITC-labeled (Cat#A24477, Invitrogen) (1:100) was added to Trastuzumab stained cells, and washed three times. All acquisitions were performed with an Attune NxT Acoustic Focusing Cytometer (Invitrogen, Thermo Fisher). Data were analyzed with FlowJo software v10.

2.7. Uptake and internalization experiments in vitro

Uptake and internalization were assessed using an Incucyte S3 live-cell analysis system (Sartorius, Goettingen, Germany). Trastuzumab antibody (obtained from the hospital pharmacy of the Regina Elena Cancer Institute as sterile preparation for therapeutic infusion) was conjugated with the pH-sensitive dye pHrodo using the Deep Red Antibody Labeling kit (#P35355, Invitrogen, Thermo Fisher scientific), according to the manufacturer's instructions. Human melanoma cells A375 (obtained from the American Type Culture Collection, ATCC) were seeded at a density of 3×10^3 cells/well in 96-well plates one day before the addition of Trastuzumab-pHrodo (10 μg/mL), alone or combined with THE-10 (1.0 mg/mL). Phase contrast and fluorescence images of cells cultured under standard conditions (37 °C, 5 % CO_2, RPMI 1640 medium, 10 % fetal bovine serum (FBS), 1 % penicillin–streptomycin and 1 % glutamine) were captured at 20× magnification every 60 min for 48 h, and mounted in the time-lapse mode by on-board software. Red fluorescence (from pHrodo-labeled antibodies internalized in acidic intracellular compartments) was elaborated by the integrated, automated Incucyte software, and quantitated after background subtraction. Data were plotted and analyzed by onboard software. Internalization was expressed as per cent of baseline (time 0) fluorescence over incubation time.

2.8. Testing of the THE-10 fusion protein activity on cultured cells: anti-proliferative effect stimulation

To assess proliferation, human melanoma A375 cells and normal human foreskin fibroblasts, HFF (obtained from the American Type Culture Collection, ATCC) were seeded at a density of 1×10^3 cells/well in 96-well plates (Costar #3595). On the following day, Trastuzumab Deruxtecan (obtained from the hospital pharmacy of the Regina Elena Cancer Institute as sterile preparation for therapeutic infusion) and THE-10 were added, alone or combined, at various concentrations (T-DXd), and at the predetermined optimal concentration of 1.0 mg/mL (THE-10). Then, cells were grown in RPMI medium, 10 % FBS (A375) or DMEM medium, 15 % FBS (HFF), under standard conditions. After 96 h of treatment, cell viability was measured by adding 100 μL of Cell Titer-Glo reagent (Promega, Madison, WI, USA) to each microtiter well (triplicate determinations). Plates were incubated for 10 min at room temperature in the dark, and luminescence was determined on a Synergy/LX multimode reader (Biotek), using the Gen5 3.10 Imager software. Results were plotted as mean ± SD, and analyzed by GraphPad Prism 9.

2.9. In vivo studies authorizations and response determination

Protocols for animal studies were approved by the Institutional Animal Care and Use Committees of the University of Udine, Italy (permission number 414/2021-PR, 11 June 2021), University of Chieti, Italy (permission number 391/2022-PR, 06 July 2022), and the Institute of Microbiology of the Czech Academy of Sciences, Czech Republic (permission number 111/2019, 16 December 2019), respectively. Experiments were compliant with the principles laid down in the European Community Council Directives (86/609/EEC) including the 3R principle.

In all experiments, tumor volume was measured twice a week with a digital caliper and mouse weight was monitored. Animals were sacrificed at the end of the study period or when the tumor had reached a volume $\geq 1000\ mm^3$. For treated groups only, the percentage of Tumor Growth Inhibition (% TGI) was defined as 100×(MTVcontrol-MTVtreated)/MTVcontrol, where MTV is the median tumor volume. THE-10 was injected before the active drugs to allow enough time for the booster THE-10 molecule to reach and accumulate at the tumor site. Based on the pharmakokinetics of THE-0504, and under the assumption that the transit time of small drugs (Gemcitabine and Irinotecan) would be much shorter than that of large macromolecules (THE-0504 nanoferritin and sacituzumab govitecan e.g. IMMU-132) the interval between injections was 24 h and 10 min respectively. Further experimental details for the in vivo studies are reported below.

2.10. In vivo anti proliferative enhancement effect of THE-10 using KPC pancreatic cancers

Seven-week-old female C57BL/6 mice (Charles River Laboratories, Lecco, Italy) were injected subcutaneously (i.e., right flank) with 0.5×10^6 pancreatic KPC cells resuspended in a 1:3 (v:v) solution of PBS:

Matrigel in a final volume of 200 μL. Three different experiments were carried-out using this cancer model.

In the first experiment, as test cytotoxic drug compound was evaluated the small molecule Gemcitabine (gemcitabine hydrochloride, MedChemExpress, USA). When tumors had reached a volume of about 100–200 mm^3, mice were randomized in groups of six animals and injected with 200 μL of physiological saline (intravenously, i.v.), 200 μL Gemcitabine (100 mg/Kg; intraperitoneal, i.p.) or 200 μL Gemcitabine (100 mg/Kg; i.p.) plus 200 μL THE-10 (130 mg/Kg; i.v.). THE-10 was injected 24 h before treatments. Mice were injected twice a week for two weeks.

In the second experiment, as test cytotoxic drug compound the large macromolecule THE-0504 nanoferritin (Thena Biotech Srl) was evaluated [21,22,26]. When tumors had reached a volume of about 200–250 mm^3, mice were randomized in groups of six animals and injected i.v. with 200 μL of physiological saline (i.v.), 100 μL THE-0504 (1.0 mg/kg), 100 μL THE-0504 (1.0 mg/kg) plus 100 μL iRGD peptide (3.0 mg/Kg; named certepetide, MedChemExpress, USA) or 100 μL THE-0504 (1.0 mg/kg) plus 100 μL THE-10 (130 mg/Kg). Assuming a fairly complete release of the 24 iRGD molecules from a single 24-mer ferritin molecule, dosages of 3.0 mg/kg of the naked iRGD peptide and 130 mg/kg of THE-10 are approximately equimolar. Mice were injected twice a week for three weeks. In the third experiment, as test cytotoxic drug compound the large macromolecule Sacituzumab govitecan (IMMU-132; cat. no. HY-132254, MedChemExpress, USA) was evaluated. When tumors had reached a volume of about 100 mm^3, mice were randomized in groups of six animals and i.v. injected with 200 μL of physiological saline (i.v.), 100 μL IMMU-132 (45 mg/Kg) or 100 μL IMMU-132 (45 mg/Kg) plus 100 μL THE-10 (130 mg/kg). THE-10 was injected 5–10 min before the treatments with IMMU-132. Mice were injected twice a week for a total of three administrations.

2.11. In vivo tumor accumulation enhancement effect of THE-10 using KPC pancreatic cancers

Tumor xenografts were generated injecting subcutaneously into C57BL/6 mice a suspension of 0.5×10^6 pancreatic KPC cells in a total volume of 200 μL of PBS and Matrigel (ratio 1:3). When xenografts became palpable (approximately 100 mm^3), animals were randomized in groups of three animals and injected intravenously with 200 μL of physiological saline, or with 200 μL of IMMU-132 (45 mg/Kg), or with 200 μL of IMMU-132 (45 mg/Kg) plus 200 μL of THE-10 (130 mg/kg). Mice were sacrificed 24 h later and fresh tumor tissues were either frozen in a cryo-embedding medium (OCT, Bio-Optica) for immunofluorescence analysis, or snap-frozen for Western blot analysis. For immunofluorescence analysis cryostat sections were incubated with the following antibodies: AlexaFluor-488 conjugated anti-human IgG (A11013, Invitrogen, Life Technologies) in order to detect IMMU-132 and rat monoclonal anti-CD31 (550,274, BD Pharmingen), mixed with rat monoclonal anti-CD105 (550,546, BD Pharmingen). Nuclei were stained with DAPI solution (Sigma). Images were acquired using a Zeiss LSM 800 confocal microscope. Detector gain voltages and pinhole were set at the beginning of the experiment and maintained constant during the acquisition of all samples. No significant fluorescent signal was detectable with the secondary antibodies alone. For Western blot analysis, snap frozen tumor tissues (200 mg) were submerged in 0.6 mL of RIPA Lysis buffer containing a protease inhibitor cocktail (Sigma-Aldrich, St. Louis, MO, USA) and a phosphatase inhibitor cocktail (Roche). Tissues were homogenized with a mechanical homogenizer (TissueRuptor II, QIAGEN GmbH, Germany), which was run for 10 s followed by a 20 s pause for six cycles. After centrifugation at 4 °C for 15 min at 10,000 rpm, supernatants were collected. Equal amounts of extracted protein as determined by the Bradford protein assay (Bio-Rad) were separated by sodium dodecyl sulfate (SDS)–10 % polyacrylamide gel electrophoresis and blotted on nitrocellulose membranes (Amersham). After blocking in 5 % non-fat milk in Tris-buffered saline with Tween-20 (TBS-T; Sigma Aldrich, St Louis, MO), IMMU-132 accumulation was detected using anti-human IgG-HRP (A0170, Sigma Aldrich) at the dilution of 1:10000. Overnight incubation with β-Actin (1:40000, A5441, Sigma-Aldrich) followed by goat anti-mouse HRP-conjugated secondary antibody (Bio-Rad, Hercules, CA, USA), was used as loading control. Blots were developed with a chemiluminescence detection system (UVITEC Cambridge).

2.12. In vivo effects of THE-10 in CT26 colorectal cancers

Eight- to ten-week-old male Balb/c mice (AnLab, Prague, Czech Republic) were subcutaneously injected with 1×10^6 syngeneic colorectal adenocarcinoma cells CT26 (ATCC, USA).

In the first experiment, when tumors reached a volume about 50–100 mm^3, animals were subdivided into groups of six animal each and injected with 200 μL of saline (i.v.) or THE-10 (120 mg/Kg) two times per week for a total of four injections. Three additional groups of five animal each were treated with 200 μL of saline (i.v.), or THE-05 (120 mg/kg) or THE-10 (120 mg/Kg), to be used for histology and immunohistochemistry analyses. These groups were sacrificed after 24 h from the last treatment and tumors collected. Details on this part are reported in the Supplementary section.

In the second experiment using colorectal adenocarcinoma cells CT26, animals were injected with 200 μL of saline (i.v.), 300 μL of irinotecan (100 mg/Kg) (i.p.) or 300 μL of irinotecan (i.p.) plus THE-10 (120 mg/Kg) (i.v.), two times per week for a total of four injections. THE-10 was injected 24 h before the treatment with irinotecan (irinotecan HCl trihydrate, MedKoo Biosciences, Inc., USA).

2.13. In vivo antiproliferative enhancement effect of THE-10 using MiaPaca2 pancreatic cancer

Four-week-old female athymic nude mice (Envigo, Italy) were injected subcutaneously (i.e., right flank) with 5×10^6 pancreatic MiaPaca2 cells resuspended in 200 μL of DMEM medium plus 1 % BSA. When tumors had reached a volume of about 80–100 mm^3, mice were randomized in groups of six animals and injected i.v. with 200 μL of physiological saline (i.v.), 100 μL THE-0504 (1.0 mg/kg), or 100 μL THE-0504 (1.0 mg/kg) plus 100 μL THE-10 (130 mg/kg). Mice were injected twice a week for three weeks.

Statistical analysis. Values are presented as the means and standard deviation. Data analysis was performed by GraphPad Prism version 5. Statistical analysis of tumor growth curve and tumors weights at the sacrifice were done using one-way ANOVA analysis, adopting the Kruskal-Wallis test and using Dunn's Multiple Comparison test for coupled comparisons. Results with confidence interval CI 95 % ($p < 0.05$) were considered statistically significant.

3. Results

3.1. Design and production of THE-10

THE-10 is a modification of our previously described HFt-MP-PASE THE-05 protein [22,36]. Scheme 1 shows the positions of functional sites, e.g. PASE, the peptide binding PD-L1 (PD-L1Pep-1), the peptide binding integrin αVβ3/αVβ5 and NRP-1 (iRGD or Certepetide), and the MP cleavage sites. BAP sequences are linear versions of two previously reported cyclic BAPs. Three-dimensional structural model of the protein macromolecule is shown in Scheme 1. THE-10 is characterized by a spherical scaffold typical of the ferritins superfamily, and by a long N-terminal domain exposed to the solvent. As expected, N-terminus is highly flexible in nature being formed by random coil structures (PASE), allowing for a high exposure of the single BAPs present in the domain to possible ligand-binding (see below and discussion).

3.2. THE-10: biochemical characterization and cleavable N-terminus

Purified (see methods) THE-10 was biochemically characterized. As expected, protein samples were highly soluble in buffer up to 150 mg/mL (not shown). Stability at 37 °C was then assessed both in buffer and in serum, and was excellent in both conditions, with no visible degradation after 18 h of incubation (Fig. S1).

Additionally, THE-10 was compared with THE-10 incubated at 37 °C for 2 h with a collagenase IV preparation containing matrix metalloproteases MMP-2 and 9. These are typically expressed in the tumor microenvironment. Size-exclusion chromatography (SEC, Fig. 1A) and sodium dodecyl sulfate–polyacrylamide gel electrophoresis (SDS-PAGE, Fig. 1B) revealed the expected differences in elution volumes and profiles before and after cleavage. The latter were slight but clearly detectable and resulted in a shift in electrophoretic band migration profiles compatible with the anticipated drop of about 10 kD in each HFt subunit. Therefore, highly purified THE-10 is cleavable, e.g. BAPs are expected to be released at the TME in the presence of MMPs.

3.3. BAP-mediated receptor binding of THE-10

To determine whether BAPs confer receptor tropism, THE-10 binding was assessed by surface plasmon resonance (SPR) using recombinant αVβ3, neuropilin-1 (NRP-1) and PD-L1 as ligands (Fig. 2A and B). In all experiments, an increase in RU relative to baseline indicates complex formation between the immobilized ligand and the analyte. The plateau region represents the steady-state phase of the interaction. The decrease in RU after 120 s (Fig. 2A) or 180 s (Fig. 2B) indicates analyte dissociation from the immobilized ligand after HST buffer injection. All measured dissociation constants (K_D) were in the nanomolar range, indicating strong binding affinity between the THE-10 analyte and its ligands. Nevertheless, the two ligands showed a different behaviour in the interaction with the functionalized construct. As shown in Fig. 2A, the interaction between the THE-10 construct and αVβ3 prompted out a strongly biphasic interaction, characterized by two association rate constants (k_{on}) and two dissociation rate constants (k_{off}). Two models are compatible with the αVβ3 SPR sensorgram: either (a) a heterogeneous ligand binding model with one analyte (THE-10) and two possible binding sites, with high and low affinity respectively (Fig. 2A); or (b) a mixed receptor population with two different binding affinities. Although kinetics does not allow to firmly distinguish between models, the first interpretation is preferred, since the amplitude of the rapid dissociation phase is increasing with increasing concentration of the analyte, indicating that higher analyte concentrations populate more easily the alternative site at lower affinity. On the contrary, PD-L1 data fit a straightforward 1:1 interaction model (Fig. 2B), with a very low K_D value consequent to the very slow k_{off} value. This indicates an extremely stable interaction between THE-10 and PD-L1. In contrast, no significant SPR response could be detected for NRP-1 ligand, (data not shown).

3.4. THE-10 enhances in vitro internalization of a therapeutic antibody

As a first step to determine whether biochemical activity translates into biological activity, THE-10 was assessed for its ability to enhance the uptake and internalization of a co-administered anti-cancer drug (booster effect). The humanized therapeutic antibody Trastuzumab (TTZ) was selected as a test compound. TTZ binds the Human Epidermal Growth Factor Receptor 2 (HER2), that is typically overexpressed in breast cancer cells of the HER2-positive subtype, but is also expressed, although at extremely low levels, in many human tumors, including melanoma cells. The melanoma cell line A375 recapitulates this typical HER2-low phenotype (Fig. S2A). Moreover, A375 displays low and moderate expression of αVβ3 and NRP-1, respectively (Fig. S2A), which makes it suitable to test booster THE-10 activity, if any.

On these premises, TTZ was conjugated to a pH-sensitive dye that turns red when the antibody is internalized into acidic intracellular vesicles. The TTZ conjugate was incubated with A375 melanoma cells growing for 48 h under standard conditions, either alone, or combined with THE-10, and non-fluorescent THE-10 alone was included as a negative control. Red fluorescence was monitored in a time-lapse (every 60 min) live cell imaging experiment (Fig. 3). Internalization kinetics, as revealed by progressive accumulation of red fluorescence, demonstrated that: (a) TTZ alone was internalized poorly and slowly, as expected; (b) in contrast, simultaneous presence of THE-10 in the culture medium accelerated uptake, and gradually enhanced red fluorescence intensity, that reached approximately four-fold the control with TTZ alone at endpoint; and (c) the curve of THE-10 alone coincided with background baseline fluorescence. Representative images are provided for visual appreciation of the THE-10 booster effect on TTZ internalization (Fig. 3B and C). In summary, THE-10 enhances cell uptake and internalization of

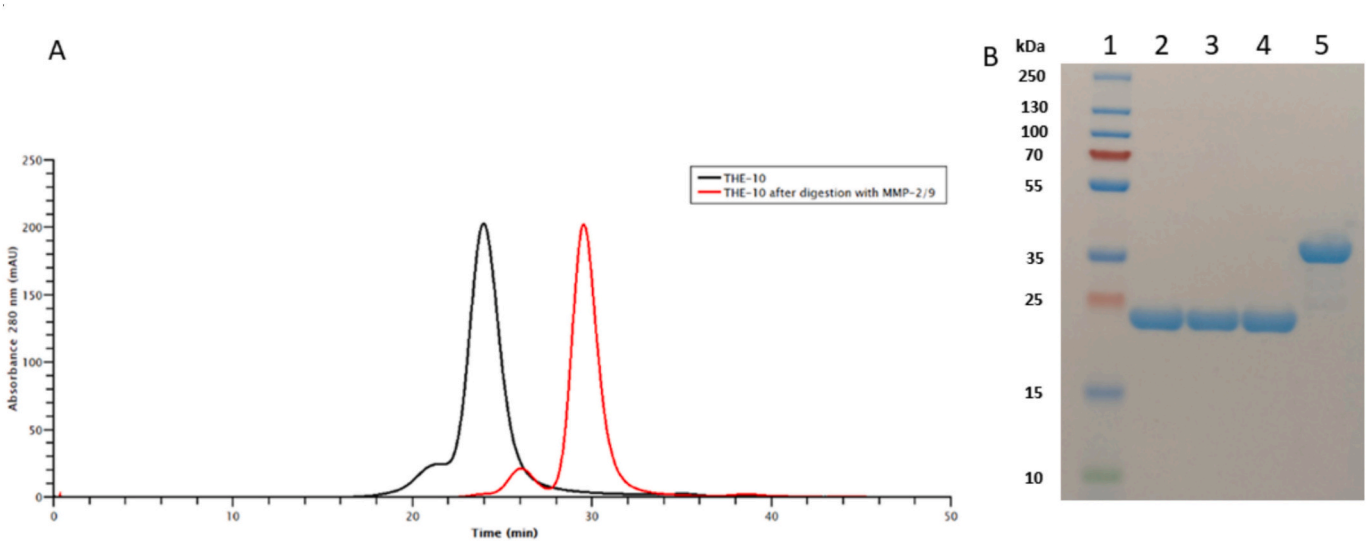

Fig. 1. THE-10 purity and polypeptides removal by tumor MMP-2/9. (A) SEC profiles of THE-10 before (black line) and after (red line) PASE and BAP sequences removal by MMP-2/9 proteinase in vitro. (B) SDS-PAGE band migration profiles of THE-10 before and after MMP-2/9 digestion. *Lane 1,* protein marker (PageRuler™ Plus Prestained Protein Ladder); *Lanes 2–4*, THE-10 (5 μg) after in vitro digestion with MMP-2/9, using different THE-10/MMPs concentration ratios: 2.5/0.25 mg/mL (*lane 2*), 1.0/0.1 mg/mL (*lane 3*) and 0.5/0.05 mg/mL (*lane 4*); *Lane 5*, THE-10 (5 μg). SDS PAGE was stained with Coomassie brilliant blue R-250.

A

$k_{on}1(M^{-1}s^{-1})$	$k_{off}1(s^{-1})$	K_D1(nM)	$k_{on}2(M^{-1}s^{-1})$	$k_{off}2(s^{-1})$	K_D2(nM)
(1.33 ± 0.04) x 10^4	(57.86 ± 0.84) x 10^{-4}	435.4 ± 20.1	(17.25 ± 0.21) x 10^4	(0.53 ± 0.13) x 10^{-4}	0.31 ± 0.1

B

k_{on} (M^{-1} s^{-1})	K_{off} (s^{-1})	K_D (nM)
(1.45±0.01) x 10^4	(4.94±0.02) x 10^{-5}	3.41 ± 0.02

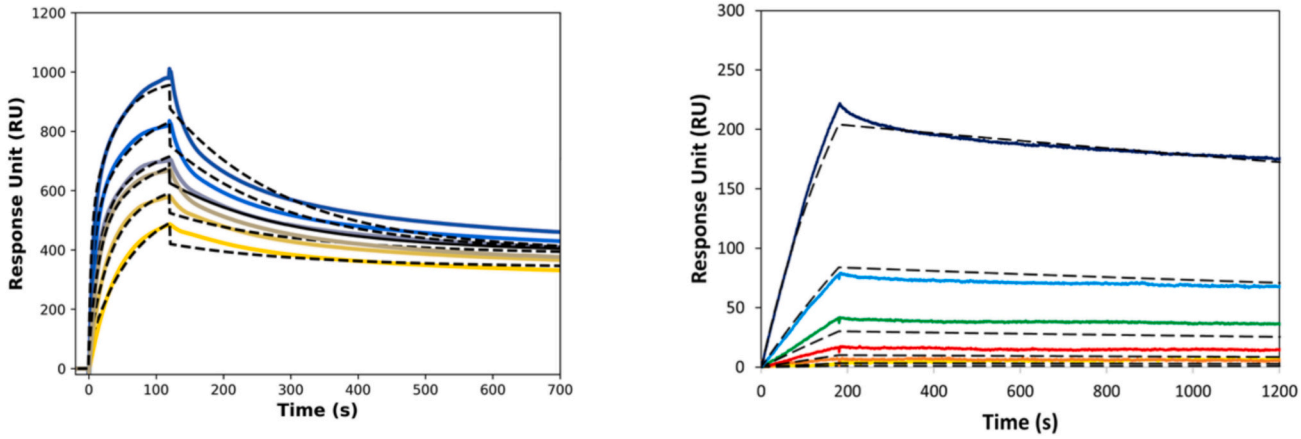

Fig. 2. Receptors binding of THE-10 by SPR experiments. *Top*: Thermodynamic and kinetic parameters of the interaction of THE-10 (analyte) with (A) human αVβ3 and (B) human PD-L1. *Bottom*: Sensorgrams show THE-10 injection in sterile HST buffer at the following molar concentrations of the 24-mer ferritin: (A): 96, 192, 384 (tested twice to ensure reproducibility of the results), 768 and 1536 nM; (B): 6.25, 12.5, 25, 50, 100 and 200 nM, followed by buffer injections to monitor analyte dissociation. In (A), curves were fitted using a heterogeneous ligand binding model. In (B), curves were fitted as single 1:1 interactions; fittings are shown as black dashed curves.

a therapeutic antibody in a cell line with the right complement of αVβ3 and NRP-1 receptors. This conclusively demonstrates functionally successful BAP grafting onto the THE-10 nanocarrier backbone.

3.5. THE-10 enhances tumor cell killing by a therapeutic Antibody-Drug Conjugate (ADC)

To determine whether increased internalization translates into improved therapeutic efficacy, the same A375 human melanoma cells were selected. They express HER2 and integrin αVβ3 at low levels, and NRP-1 moderately (Fig. S2A), showing that they have the right complement of target molecule and BAP internalization receptors. A375 cells were exposed to a derivative of the TTZ antibody, e.g. Trastuzumab deruxtecan (T-DXd), that carries a toxic topoisomerase I inhibitor. T-DXd was selected because, unlike other naked antibodies and ADCs, it has remarkable unprecedented activity on HER2-low breast cancers [38], although results of clinical trials with HER2-low cancers from other histotypes are not yet available.

T-DXd killing of A375 melanoma cells was dose-dependent. At the lowest T-DXd dosage THE-10 enhanced killing approximately four times, whereas THE-10 alone displayed no significant effect as compared to medium alone (Fig. 4A). As a control, normal human foreskin fibroblasts (HFF) were selected. These lack detectable HER2 and integrin αVβ3 receptor expression, although they do display moderate expression of NRP-1 (Fig. S2B), which results in a double-defective phenotype negative for both the target HER2 molecule and one of two crucial internalization receptors. Testing under the same conditions used for A375 melanoma cells revealed that T-DXd-mediated killing was appreciable at high concentrations, but at the lowest concentrations it was marginal and at least 4 times lower than melanoma killing, as expected. Most importantly, THE-10 exerted no booster effect regardless of T-DXd concentration (Fig. 4B).

Therefore, THE-10 mediates a booster effect on a cytotoxic antibody to HER2 in a melanoma cell line expected to be unresponsive to anti-HER2 treatments but capable to internalize the antibody in presence of THE-10. In contrast, normal fibroblasts are far less sensitive to T-DXd, and completely refractory to boosting, which demonstrates that THE-10 enhances tumor-selectivity of T-DXd, as intended.

3.6. THE-10 slows tumor growth in a colorectal cancer mouse model through immune cell infiltration

A PD-L1 peptide (PD-L1pep1) fused to the N-terminal of the native human ferritin (HFt) was previously reported to block PD-1/PD-L1 interactions, inhibit the immune suppressive activity of PD-L1 and have moderate antitumor effects in vivo [39]. A similar peptide was incorporated into THE-10, the only difference being the absence of the terminal N- and C-terminal cysteine residues. The antitumor activity of THE-10 was directly assessed in CT26 mouse colon cancer allografts, e.g. the same syngeneic tumor model selected by Jeon IS et al., in light of high PD-L1 expression [39]. Established allografts were treated by intravenous injection of either THE-10 (120 mg/kg) or saline two times per week for a total of four injections. Treatment with THE-10 mildly inhibited tumor growth compared with control mice treated with saline (Fig. 5A). Although mild, this antitumor effect is in line with the original report [39]. No significant differences in body weight were observed among experimental groups during treatment (not shown), suggesting limited if any adverse effects. Immunohistochemical analysis of tumor immune infiltrates demonstrated significant accumulation of CD3+ and CD8+ effectors in the TME only for the mice treated with THE-10 (Figs. 5B–E, and S3 and S4). These results confirm that BAP grafting confers ICI-like properties to THE-10 most notably a canonical accrual of immune effectors at the tumor site.

3.7. THE-10 enhances the in vivo antitumor activity of two small drugs: irinotecan and gemcitabine

Irinotecan and gemcitabine are two key drugs employed worldwide for the treatment of several solid tumors. However, therapeutic resistance, short half-lives, and side effects owing to toxicity limit their success in clinical practice. For this reason, we examined the ability of THE-10 to boost drug accumulation and anticancer effects in two murine

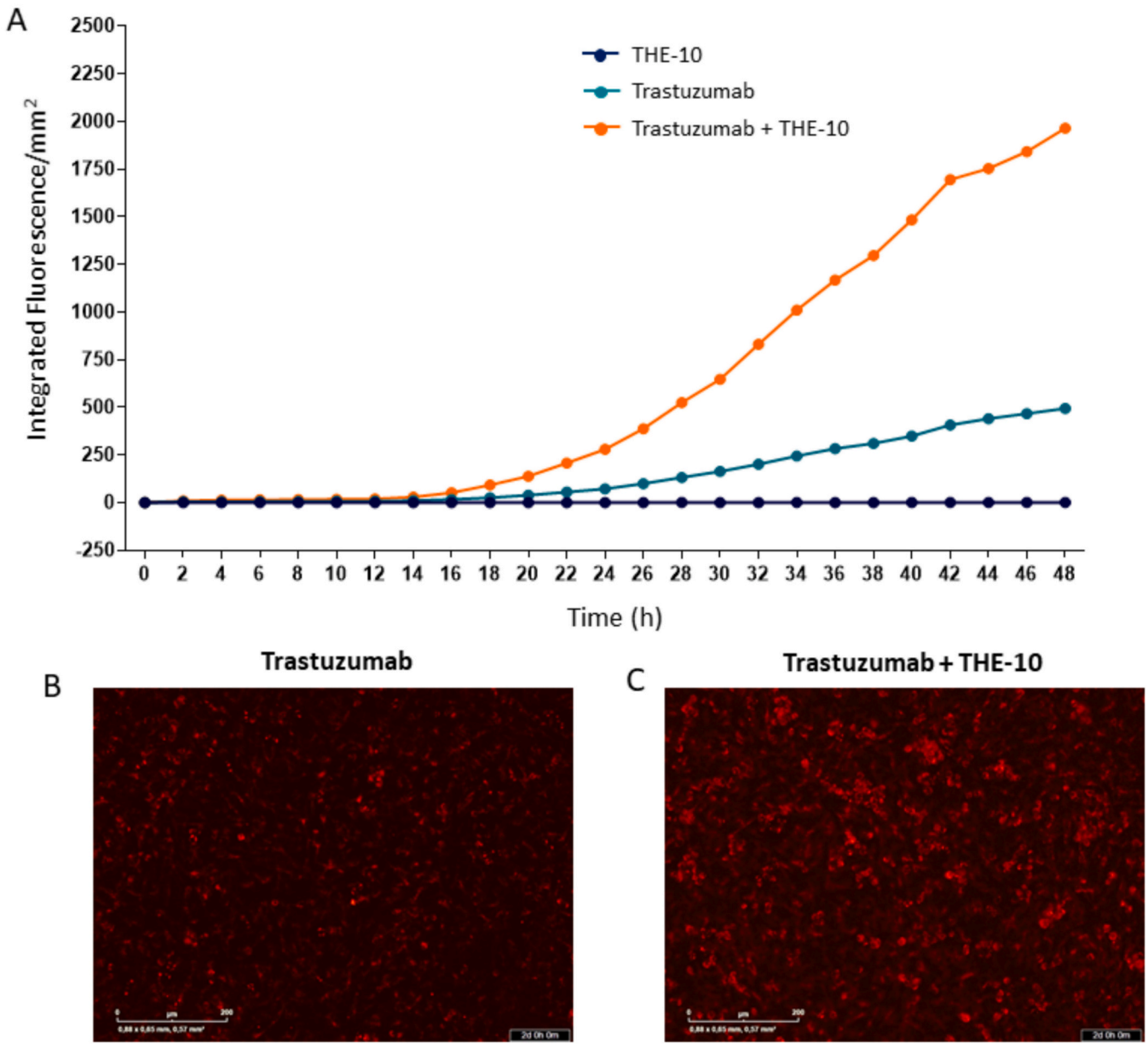

Fig. 3. Kinetics of antibody Internalization by A375 melanoma cells. A375 cells were treated with pHrodo Deep Red labeled Trastuzumab (10 μg/mL), alone or combined with THE-10 (1 mg/mL), and with THE-10 alone as a no-fluorescence control. Treatment was for 48 h in an Incucyte Live-Cell system. (A) A time course of red Integrated Fluorescence, e.g. fluorescence captured by the built-in camera in the microscopic field at 20× magnification. Fluorescence intensity is proportional to the amounts of antibody internalized into acidic intracellular vesicles. Integrated fluorescence, calculated by the Incucyte on-board software is displayed for the three testing conditions, following acquisition at 60 min intervals. Each point of the internalization kinetic represents the mean of 18 independent readings of 2 wells, which makes standard deviation negligible (bars not shown because comprised within the dot size). All three curves diverge significantly (2way ANOVA test $p > 0.001$) from the 24 h time point. Integrated fluorescence of THE-10 is superimposable with the curve generated with medium alone, that is not shown due to complete overlap. (B and C) Red images captured at time 48 h post treatment. Bar: 200 μm.

models. The anticancer booster effect of combination therapy with irinotecan plus THE-10 was evaluated in the syngeneic mouse colon (CT26) cancer model (Fig. 6A), since irinotecan represents a standard therapy for this type of tumor. Four intravenous injections of THE-10 (120 mg/kg), followed by intra-peritoneal injections of irinotecan (100 mg/kg), two times per week for a total of four injections, significantly reduced tumor growth as compared to injection of the sole Irinotecan ($p<0.05$; Fig. 6A). Tumor Growth Inhibition (TGI) was 29.0 % for the Irinotecan-treated group and 63.0 % for the group treated by irinotecan plus THE-10 (Table 1).

For gemcitabine evaluation, a pancreatic model was used since this small drug represents a gold-standard chemotherapy agent in advanced pancreatic cancer. Similarly to irinotecan, co-administration of THE-10 (130 mg/Kg) with gemcitabine (100 mg/Kg) decreased growth of a syngeneic mouse pancreatic (KPC) tumor significantly more than gemcitabine monotherapy ($p<0.001$, Fig. 6B), with TGI values of 82.2 % vs 48.8 % (Table 1).

3.8. THE-10 enhances the in vivo antitumor activity of the nanoferritin THE-0504 in two different models of pancreatic cancer

THE-0504 is a complex based on THE-05, a genetically modified human ferritin which acts as a drug carrier. THE-0504 encapsulates in its cavity, as payload, the cytotoxic drug Genz-644282, a non-camptothecin

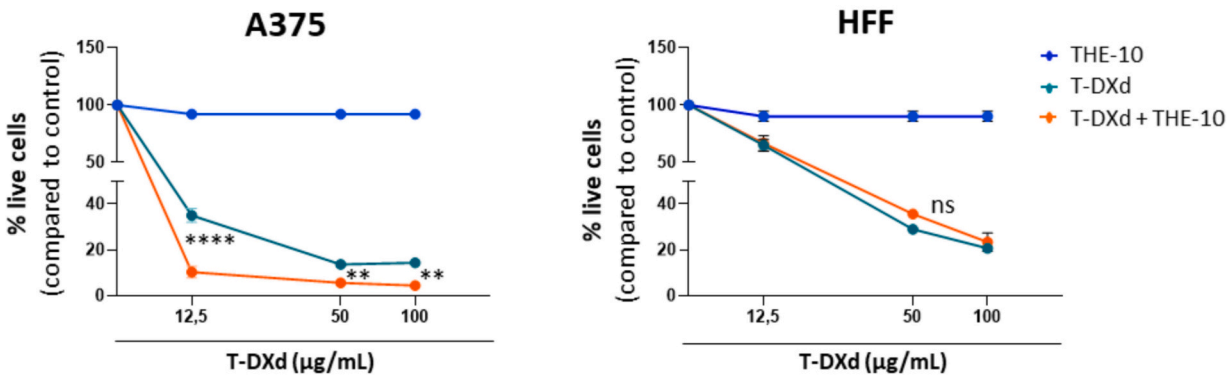

Fig. 4. Booster effect of THE-10 on melanoma cells (A375) and normal human foreskin fibroblasts (HFF). Cell killing of the two cell lines was measured after 5 days of treatment with THE-10, Trastuzumab deruxtecan (T-DXd), or both, as indicated (color-coded lines). Where present (blue line), THE-10 was used at 1 mg/mL, whereas T-DXd (green and red lines) was used in a dose-response experiment at the three concentrations noted in abscissae. All data are expressed after normalization to 100 % (no killing in control cultures grown in medium alone). Each experimental condition was performed in triplicate. Bars correspond to mean ± SD from 3 replicates per condition. Standard deviation is shown (bars). Statistical differences (2way ANOVA test): ****$p < 0.0001$: T-DXd vs T-DXd + THE-10 (12.5 µg/mL), **p 0.0094: T-DXd vs T-DXd + THE-10 (50 and 100 µg/mL); ns: not significant.

topoisomerase-I inhibitor. Recently, we evaluated THE-0504 in solid tumor animal models. Delayed tumor growth and durable complete remissions were observed in combination with a manageable toxicity profile [21,22,37]. THE-0504 is currently at an advance development stage for first-in-human trials in solid tumors.

This prompted us to evaluate THE-10 as an antitumor booster of THE-0504. To this end, a murine model of pancreatic cancer was selected in which the activity of THE-0504 is very low, since THE-0504 binds the murine CD71 receptor much less than its human receptor orthologue [26]. Syngeneic mouse pancreatic (KPC) cancers, about 250 mm^3 in volume, were treated by intravenous injection twice a week for three weeks. Mice received 200 µL of physiological saline, or THE-0504 (1.0 mg/kg), or THE-0504 (1.0 mg/kg) plus iRGD peptide (3.0 mg/Kg), or THE-0504 (1.0 mg/kg) plus THE-10 (130 mg/kg). Under these conditions, the naked iRGD peptide and THE-10 are provided in equimolar amounts. Tumor growth curves show the expected low antitumor activity of THE-0504 alone, a limited booster effect of the original cyclic iRGD peptide (CRGDKGPDC) that is currently in phase 2 clinical trial for pancreatic cancer (NCT05042128), and a much greater, and remarkable, boost by THE-10 (Fig. 7), as quantitatively estimated by TGI values (Table 1). Since the plasma half-lives of iRGD and parental THE-05 are 15 min and about 40 h respectively [37,40], these findings are consistent with a longer serum persistence and/or higher tumor accumulation/release of BAPs fused to HFt as compared to naked peptides.

The booster effect of THE-10 was assessed in a second pancreatic cancer model, that is instead susceptible to THE-0504. In this case, the tumor (MiaPaca2) was of human origin and was grown as a xenograft. Mice were intravenously injected twice a week for three weeks with 200 µL of physiological saline, THE-0504 (1.0 mg/kg), or THE-0504 (1.0 mg/kg) plus THE-10 (130 mg/kg). As shown in Fig. 8, THE-0504 alone greatly reduced tumor growth ($p < 0.001$), but despite this marked effect, addition of THE-10 resulted in a remarkable boost, revealed by an almost complete stall in tumor growth (Fig. 8A, Table 1). This is best appreciated by considering the dramatic reduction (approximately four-fold) in the weight of residual tumor masses excised from the animals at the end of the experiment compared with THE-0504 alone (Fig. 8B).

3.9. THE-10 enhances the in vivo antitumor activity of the Antibody-Drug Conjugate Sacituzumab govitecan in a murine model of pancreatic cancer

Sacituzumab govitecan (previously known as IMMU-132) is a first-in-class ADC that depends in its activity on the expression of the Trophoblast cell surface antigen-2 (Trop-2). IMMU-132 is indicated for the treatment of metastatic triple-negative breast cancer and metastatic urothelial cancer [41].

To test THE-10 boosting on IMMU-132 antitumor activity, the same murine pancreatic cancer graft (KPC) was selected, used in previous experiments. In this model, the activity of IMMU-132 alone was expected to be absent or very low due to the lack of detectable Trop-2 expression in mice [42]. Then, mice were intravenously injected three times, one every 3–4 days, with 200 µL of physiological saline, IMMU-132 (30.0 mg/kg), or IMMU-132 (30.0 mg/kg) plus THE-10 (130 mg/Kg). THE-10 was injected about 5–10 min before IMMU-132.

As expected, IMMU-132 did not exert any significant therapeutic effect, whereas in combination with THE-10 it resulted in an excellent anticancer activity, with a remarkable TGI of 93.0 %, supported by reduction in residual tumor masses (Fig. 9, Table 1). Moreover, sacituzumab was not detectable by immunohistochemistry and western blot in tumor tissues after 24 h from first injection, but became detectable upon combined treatment with THE-10 (Fig. S5).

4. Discussion

The present study describes a novel BAP-fusion protein nanocarrier based on human HFt, named THE-10. Some of the unique THE-10 anticancer features are not novel, e.g. they were inherited from protein domains already present in either the natural HFt nanoparticle or the parental nanocarrier HFt-MP-PASE (THE-05). These include an elective HFt tropism for iron-hungry, actively proliferating tumor cells, reduced CD71 binding, long circulating half-life, and activation in the TME upon conditional MMP proteolytic cleavage. These features have been extensively characterized in previous THE-05 studies [21,25,36], and were conserved in THE-10, as shown herein by either direct testing (biochemical characterization and tumor accumulation data in Figs. 1 and S5), or indirect assessment (widespread anti-tumor effects on human and mouse tumor grafts and immunohistochemistry in Figs. 3–9, S3 and S4).

Besides these pre-existing features, THE-10 incorporates novel and unprecedented add-ons, which were tested in greater detail. Unlike THE-05, that exploits the cargo properties of the HFt cavity for the controlled delivery of a cytotoxic agent, THE-10 leverages the resilience of the outer HFt shell, in that it features two releasable BAPs at a position next to the PASylation and MMP cleavage sites. This position was previously shown to be permissive to amino acid substitution, and hence it was not expected to impair folding and stability, a prediction that could be confirmed experimentally (Figs. 1, 2 and S1). These data outline how nanoparticles allow for the multiple degrees of freedom and modular design necessary to introduce dedicated add-ons in a pre-existing

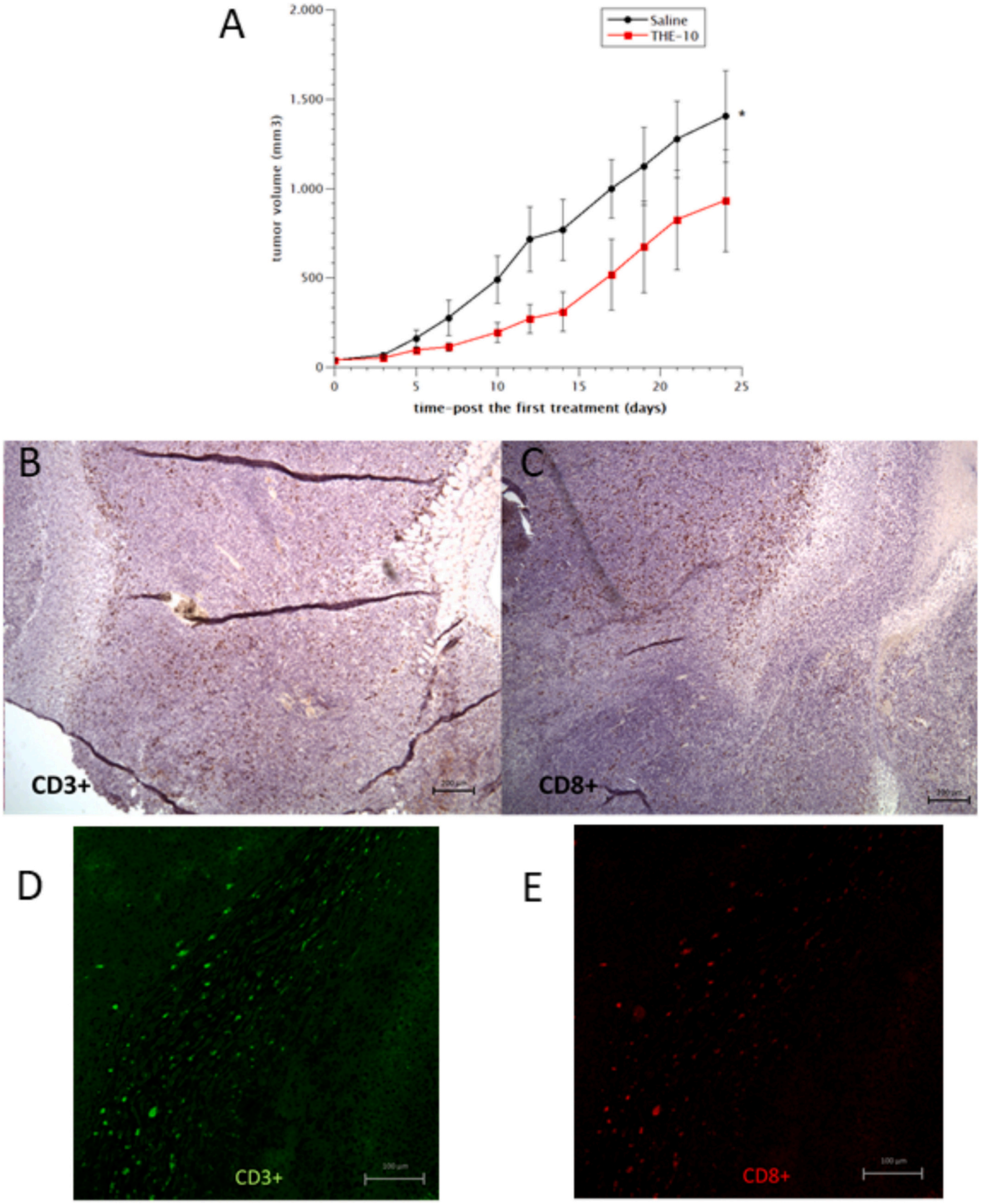

Fig. 5. THE-10 antitumor effect on CT26 syngeneic mouse colon tumors. (A) Growth curves representing the median of the tumor volume for each of the treated groups ± SEM (CI 95 %, *$p < 0.05$, *t*-test). (B, C) CD3 and (D, E) CD8 cell infiltrate in tumors treated with THE-10. The T lymphocyte infiltration was evidenced by immunohistochemistry staining with anti-mouse CD3 and CD8 antibodies in transmission light microscopy (B, D, brown dots) or by fluorescent staining in confocal microscopy (C, E, green or red dots). Representative images. 40× magnification. Bar: 200 μm.

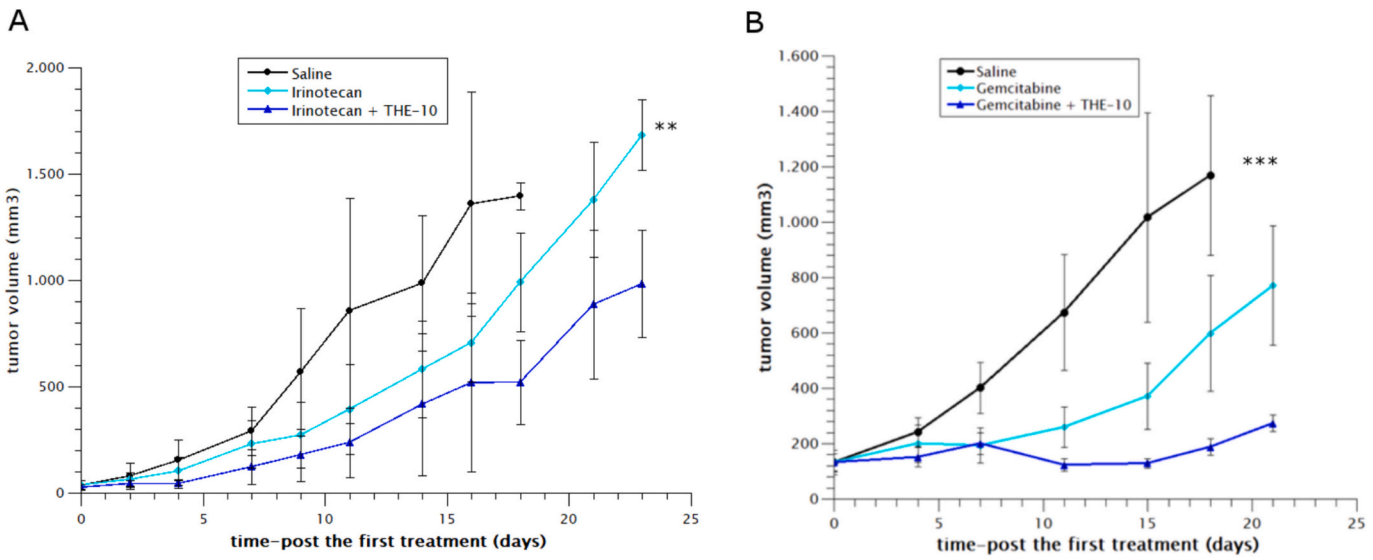

Fig. 6. Tumor treatment studies involving co-administration of THE-10 with irinotecan or gemcitabine. (A) Tumor growth curves of irinotecan and THE-10 combination therapy in CT26 colorectal cancer model. (B) Tumor growth curves of gemcitabine and THE-10 combination therapy in KPC pancreatic cancer model. Statistical differences (*t*-test) are as follows (CI 95 %). *$p < 0.05$: Irinotecan vs control, Irinotecan plus THE-10 vs control, Gemcitabine vs control, Gemcitabine plus THE-10 vs control; **$p < 0.001$: Irinotecan vs Irinotecan plus THE-10; ***$p < 0.0001$: Gemcitabine vs Gemcitabine plus THE-10.

Table 1
Summary of the combination therapy of several drugs plus THE-10 in tumor-bearing mice models reported as Tumor Growth Inhibition percentage.

Tumor model	Drug type/combo Tumor Growth Inhibition (TGI)	
Colorectal	Irinotecan	Irinotecan + THE-10
(murine, CT26)	*29.0 %*	*63.0 %*
Pancreatic	Gemcitabine	Gemcitabine + THE-10
(murine, KPC)	*48.8 %*	*82.2 %*
Pancreatic	THE-0504	THE-0504 + THE-10
(murine, KPC)	*9.4 %*	*74.2 %*
Pancreatic	THE-0504	THE-0504 + iRGD peptide
(murine, KPC)	*9.4 %*	*23.5 %*
Pancreatic	THE-0504	THE-0504 + THE-10
(human, MiaPaca2)	*82.5 %*	*98.3 %*
Pancreatic	IMMU-132	IMMU-132 + THE-10
(murine, KPC)	*0 %*	*93.0 %*

protein backbone.

THE-10 structural integrity is mirrored by conserved BAP functions. SPR receptor-binding in vitro experiments clearly show that the 2 BAPs grafted onto the THE-10 fusion nanocarrier retain their ability to bind cognate receptors αVβ3 and PD-L1 (Fig. 2). Of note, binding was demonstrated using the intact THE-10 compound and not its cleaved counterpart, that is generated in the TME upon digestion by the tumor-restricted proteases MMP-2 and 9. In this respect, receptor binding by intact THE-10 mimics the worst scenario that may possibly occur in vivo in case of negligible or absent expression of tumor MMPs (Fig. 2). Fully in agreement with structural predictions (model in Scheme 1), the PASE polypeptide is expected to fold into a random-coil, flexible structure, that is highly unlikely to fully shield single linear peptide sequences grafted in frame onto the protein N-terminus.

On the other hand, intact THE-10 did not detectably bind NRP-1 in SPR experiments. This was also expected, because binding of THE-10 to NRP-1 requires the specific cleavage of the iRGD peptide incorporated in the THE-10 construct, with the consequent exposure of the internal RGDK binding motif (C-end rule). Unfortunately, since the TME protease responsible for RGDK unmasking in vivo is unknown, it was impossible to model the C-end rule in vitro by SPR experiments. Regardless, this result indirectly supports the idea that THE-10 does not bind NRP-1, and BAPs are expected to remain 'locked in' until the nanocarrier reaches the TME.

In summary, to the best of our knowledge, THE-10 is therefore the first multi-BAP nanocarrier containing both active PD-L1-binding and iRGD-like peptides. It will be of considerable interest to compare THE-10 performance with alternative nanocarriers based on other chemistries (e.g. liposomes), once these will become available. However, serious methodological problems may arise since synthetic nanocarriers must be manufactured by production pipelines not easily 'exportable' form the originating lab, may incorporate multiple functional modules, and their dynamics of in vivo delivery (e.g. pharmacokinetics and pharmacodynamics) may not be easily controlled, complicating comparisons. Most likely, nanocarriers (more than other biomolecules) may not be reliably compared by simple bibliographic search, but exchange and parallel multi-site testing will be necessary, involving sharing of commercially available preparations, or academic exchange and collaborative efforts.

Also based on these considerations, when moving into complex in vivo testing our major aim was to measure THE-10 activity relative to robust reference standards. We elected to focus on comparisons between the naked BAPs and THE-10, since the former may be formulated as simple, homogeneous, soluble, and chemically stable preparations. Moreover, ICI-like and booster effects were tested, whenever possible, in the same experimental model that had been selected in the original BAP descriptions. With this conservative approach, cogent evidence could be provided that at least in some models THE-10 is superior to naked BAPs, and the difference may be considerable, up to 3 times in efficacy experiments (Fig. 7 and Table 1). However, the inevitable downside of this model-oriented study design is that boosting and ICI-like effects were assessed individually, and no evidence is provided herein that all the effects and safe-locks operate simultaneously and on the same tumor target. Further studies are warranted aimed at detecting possible additivity and/or synergy.

Limitations notwithstanding, this report provides to our knowledge the first proof of principle that a single BAP protein nanocarrier may deliver and/or boost the effects mediated by three major classes of antineoplastic agents: ICI, cytotoxic antibodies or nanocarriers, and small drugs. From a functional viewpoint, the two BAPs induced ICI-like effects and enhanced the antitumor activity of co-administered drugs ('booster' effect), as shown in Figs. 3–9 and S3–S4. The direct recruitment of immune effectors at the tumor site, e.g. TME conversion into a hot pro-immune milieu provides a straightforward interpretation for ICI-

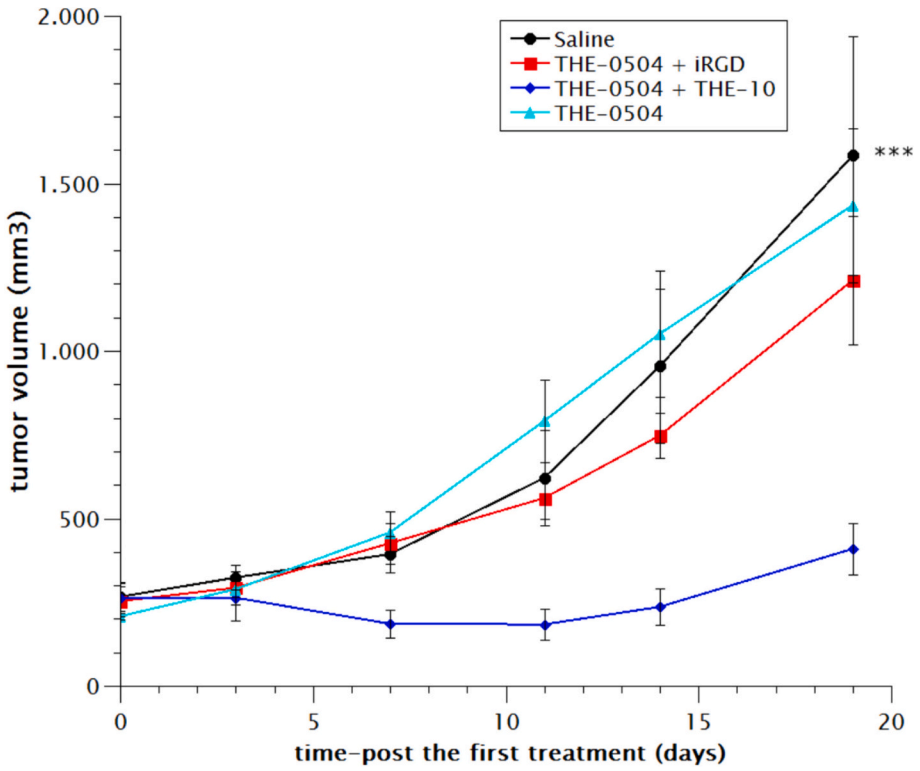

Fig. 7. Tumor treatment studies involving co-administration of THE-0504 drug with THE-10 or iRGD peptide. Tumor growth curves in KPC pancreatic cancer model. Statistical differences (*t*-test) are as follows (CI 95 %). $^{**}p < 0.001$: THE-0504 vs control, THE-0504 plus THE-10 vs control, THE-0504 plus iRGD vs control; $^{***}p < 0.0001$: THE-0504 plus THE-10 vs THE-0504 plus iRGD.

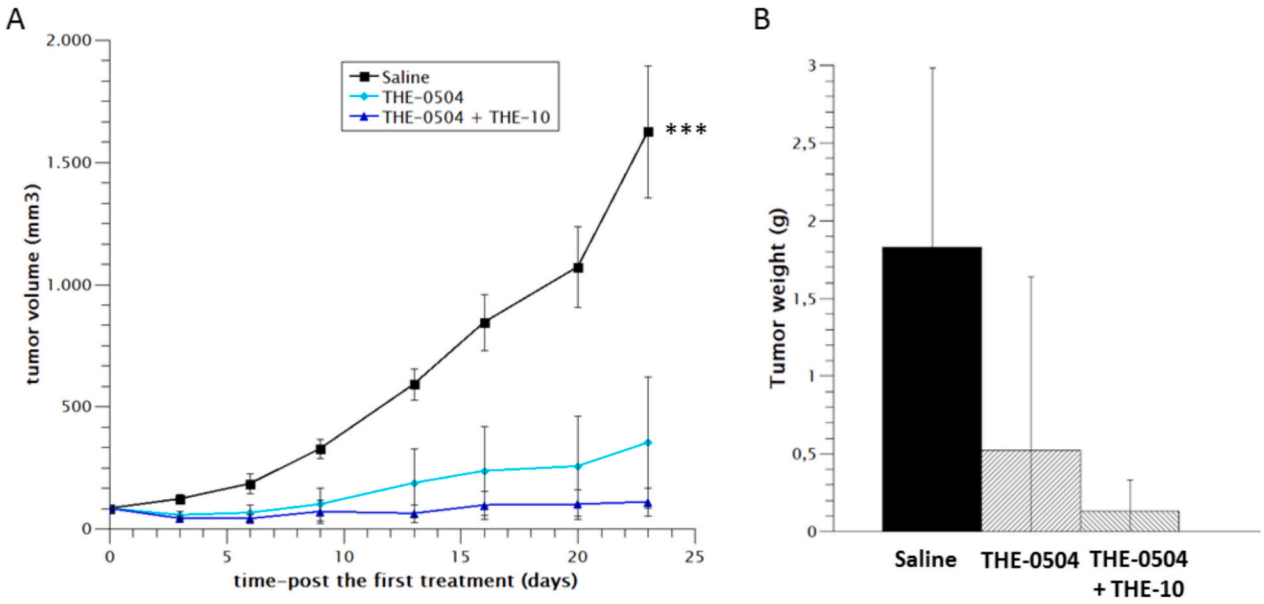

Fig. 8. Tumor treatment study involving co-administration of THE-0504 drug with THE-10 or iRGD peptide. (A) Tumor growth curves in MiaPaca2 pancreatic cancer model. (B) Tumor weights of animals sacrificed at the end of the experiment. Statistical differences (t-test) are as follows (CI 95 %). $^{**}p < 0.001$: THE-0504 vs control; $^{***}p < 0.0001$: THE-0504 plus THE-10 vs control.

like effects (Figs. 5 and S3–S4). Although the interpretations of THE-10 boosting are more complicated, this effect is potentially more intriguing because it was seen in vitro and in vivo with very diverse classes of anticancer agents, including two ADCs (T-DXd and IMMU-132), the parental nanocarrier in the same therapeutic class (THE-0504), and two small molecules (gemcitabine and irinotecan), possibly with a preferential effect on large macromolecules (Figs. 3–9). These data support the idea that THE-10 can be considered agnostic to the modality of the companion anti-tumor therapy. Also of interest, BAP-mediated boosting was not seen at all in human fibroblasts (Fig. 4). Like many other normal cells, fibroblasts express low, if any at all, T-DXd-reactive HER2, but also fail to express the full integrin/NRP-1 receptor complement that mediates T-DXd internalization through the iRGD C-end rule (Fig. S2B). Additionally, normal fibroblasts in culture are likely lacking the

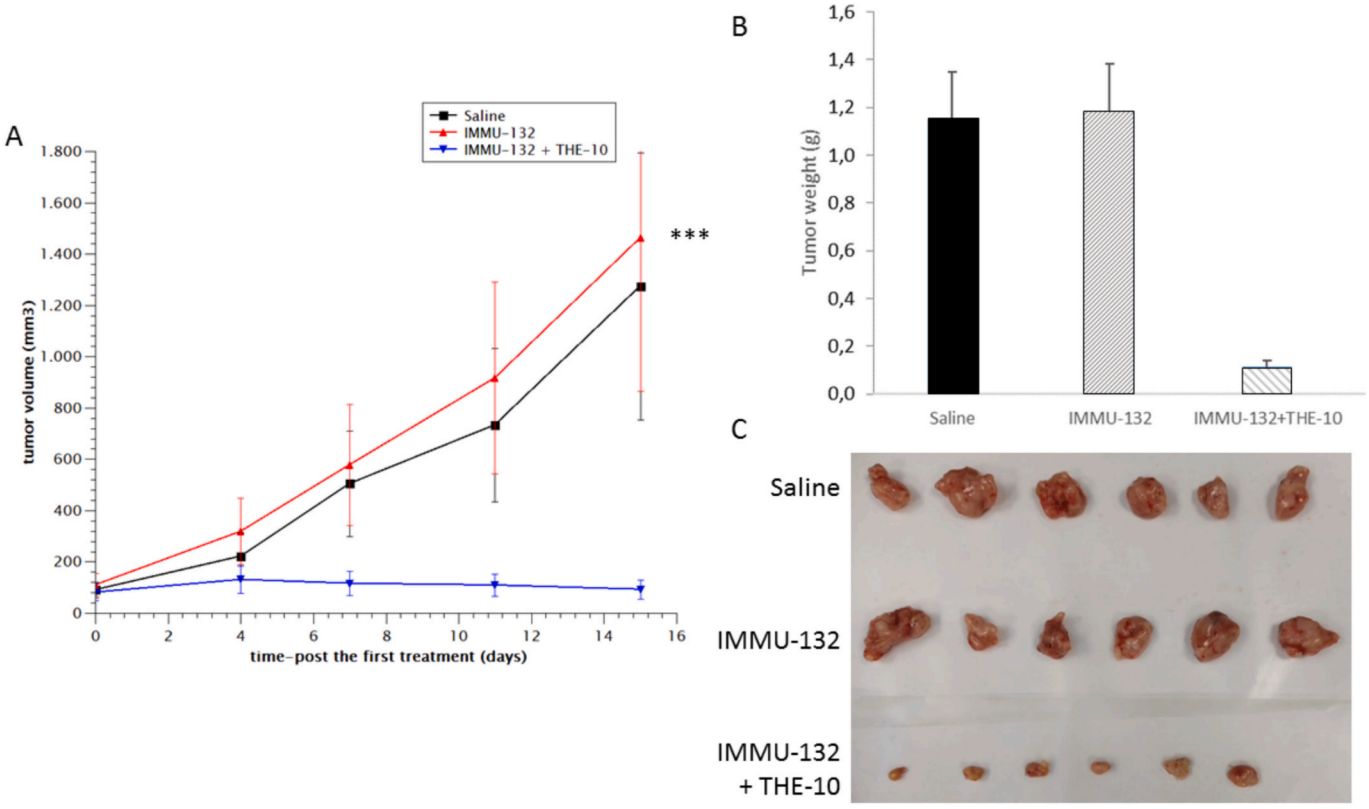

Fig. 9. Tumor treatment study involving co-administration of Sacituzumab govitecan (IMMU-132) with THE-10. (A) Tumor growth curves of IMMU-132 and THE-10 combination therapy in KPC pancreatic cancer model. (B) Tumor weights and images from animals sacrificed at the end of the experiment. Statistical differences (*t*-test) are as follows (CI 95 %). $^{**}p < 0.001$: IMMU-132 vs control, IMMU-132 vs IMMU-132 plus THE-10; $^{***}p < 0.0001$: IMMU-132 plus THE-10 vs control.

unknown TME-resident protease that linearizes iRGD exposing its C-terminus. Then, it appears that THE-10 exerts a triple-check on drug delivery and boosting: (a) selective targeting (preferential binding to tumor-expressed CD71 or PD-L1), (b) targeted delivery (conditional MMPs cleavage in the TME), and (c) BAP-dependent activation (subordination of therapeutic boosting to the C-end rule). Three-fold control is highly desirable to spare normal cells, since THE-10 is versatile, and co-administration of anticancer compounds as diverse as ADCs and

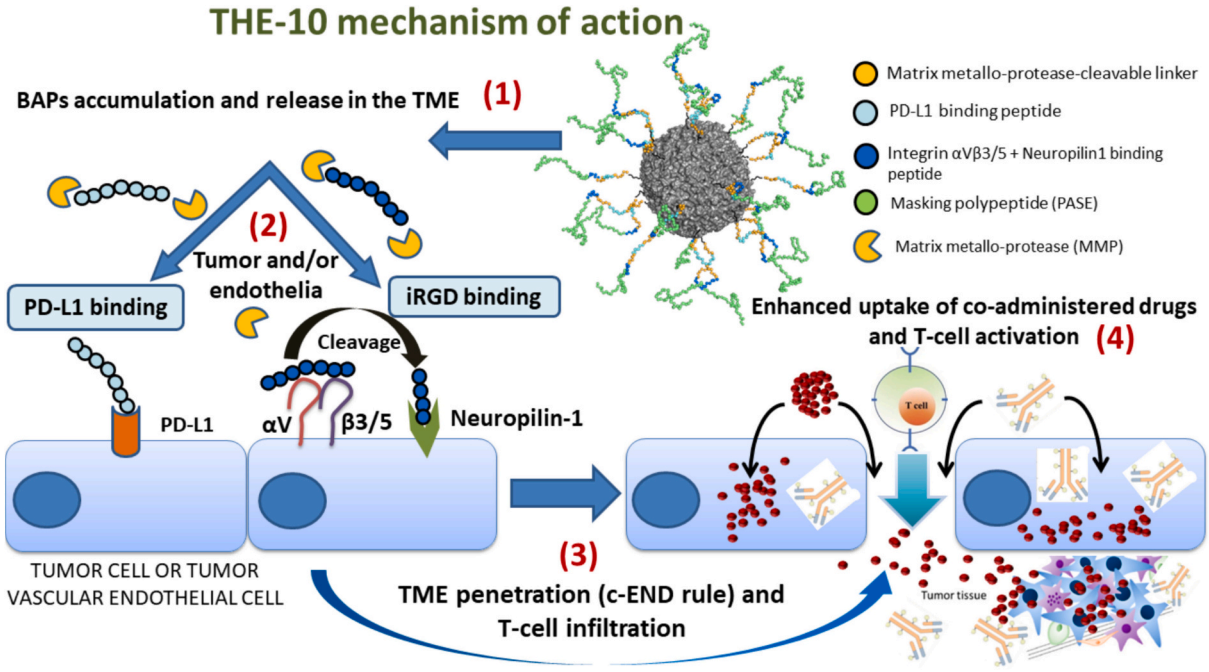

Scheme 2. Hypothetical mechanism of action for the THE-10 compound. After accumulation in the Tumor Micro-Environment (TME), BAPs are proteolytically released from the external surface of THE-10, bind their specific receptors, and activate drug penetration and T-cell function downstream.

chemotherapeutic agents may result in a complex and difficult to anticipate toxicity spectrum. Accordingly, no toxic effects including body weight loss were evident in any of the tumor-bearing mice treated with THE-10, suggesting that boosting therapeutic effects did not appreciably worsen associated side/adverse effects. However, our studies were not specifically designed to capture toxicological and toxicokinetic profiles, which will have to be assessed in future, adequately powered studies in appropriate animal hosts.

Based on the available data (previous BAP descriptions and herein), the hypothetical 4 steps underlying cytotoxic and immune boosting by THE-10 are depicted in Scheme 2, highlighting how HFt-like nanocarriers may optimize and boost therapeutic synergies.

If supported by favorable efficacy and toxicity profiles, multi-BAP nanocarriers such as THE-10 may find application when drugs under clinical development fail to clearly meet efficacy endpoints and, in a broader perspective, to redefine the idea itself of drug repositioning. A two-BAP THE-10 nanocarrier may combine pro-immune and booster effects to: (a) candidate for treatment tumors that are currently considered pharmacologically insensitive to one or more drugs (T-DXd and melanoma is a case in point), and tumors that adaptively become insensitive to either ICI or small molecules during treatment; (b) increase the number of therapy lines potentially available for a given disease setting; (c) increase the number of drug combinations and sequences, optimizing and expanding synergistic effects; and (d) more effectively manage associated side effects, e.g. by reciprocally decreasing/tuning/adjusting the dosages of THE-10 and one or more co-administered drugs.

CRediT authorship contribution statement

Giada Tisci: Investigation, Formal analysis, Conceptualization. **Lenka Rajsiglova:** Methodology, Investigation, Formal analysis, Conceptualization. **Sandra Bibbo:** Investigation, Formal analysis. **Giovanna Zicchedu:** Methodology, Formal analysis. **Elena Ricciardi:** Formal analysis. **Elisabetta Falvo:** Resources, Methodology, Conceptualization. **Vincenzo De Laurenzi:** Resources. **Gianluca Sala:** Writing – original draft, Resources, Project administration, Methodology, Data curation, Conceptualization. **Emily Capone:** Formal analysis. **Gianni Colotti:** Resources, Investigation, Formal analysis. **Alessandro Arcovito:** Formal analysis. **Noah Giacon:** Formal analysis. **Peter Makovický:** Formal analysis. **Leonid Sushytskyi:** Formal analysis. **Pavol Lukac:** Formal analysis. **Luca Vannucci:** Writing – original draft, Resources, Methodology, Investigation. **Patrizio Giacomini:** Writing – original draft, Project administration, Investigation, Conceptualization. **Pierpaolo Ceci:** Writing – original draft, Project administration, Methodology, Investigation, Data curation, Conceptualization.

Declaration of competing interest

The authors declare the following financial interests/personal relationships which may be considered as potential competing interests: Pierpaolo Ceci reports financial support was provided by National Research Council. Gianluca Sala reports financial support was provided by Gabriele d'Annunzio University of Chieti and Pescara. Vincenzo De Laurenzi reports financial support was provided by Gabriele d'Annunzio University of Chieti and Pescara. Gianni Colotti reports financial support was provided by National Research Council. Luca Vannucci reports financial support was provided by Institute of Microbiology Czech Academy of Sciences. Pierpaolo Ceci and Elisabetta Falvo have patent #PCT/IB2015/057448 licensed to Thena Biotech srl. Patrizio Giacomini and Pierpaolo Ceci are Members of the Scientific Board of Thena Biotech Srl. They received no compensation or payments from Thena Biotech If there are other authors, they declare that they have no known competing financial interests or personal relationships that could have appeared to influence the work reported in this paper.

Acknowledgements

This study was partially supported by grants from the European Union Next-Generation EU within the MUR National Recovery and Resilience Plan [NRRP] - M4C2 - Action 1.1, Call "PRIN 2022" (id. 2022WC7BL2, CUP B53D23016520006 to E.F.); from the project PRIN MUR 2022HYF8KS to G.C.; from the European Union - Next Generation EU-NICR, Programme EXCELES, reg. n. LX22NPO5102 (CZ); from the Ministry of Health of the Czech Republic, project NU23-08-00071; from the RVO 61388971 of the Institute of Microbiology AS CR (institutional grant); from Fondazione-AIRC to G.S. (grant code: IG 2021 id 25696); from Ministry of Health, Italy to V.D.L. (grant code: PNRR-MAD-2022-12376202). We also acknowledge CNCCS s.c.a.r.l. (National Collection of Chemical Compounds and Screening Center, www.cnccs.it); PNRR M4C2 - Dalla ricerca all'impresa - 3.1: Fondo per la realizzazione di un sistema integrato di infrastrutture di ricerca e innovazione "Potentiating the Italian Capacity for Structural Biology Services in Instruct-ERIC (ITACA.SB)" CUP: B53C22001790006; PNRR PE8 Age-IT, co-funding from Next Generation EU [DM 1557 11.10.2022], in the context of the National Recovery and Resilience Plan, Investment PE8 – Project Age-IT: "Ageing Well in an Ageing Society"; Consiglio Nazionale delle Ricerche - CNR project DBA.AD005.225-NUTRAGE-FOE2021. Dr. Italia Falcone (IRCCS Regina Elena National Cancer Institute) and Dr. Patrizio Di Micco (Italian National Research Council CNR, Italy) are gratefully acknowledged for help with normal human fibroblast cultures and three-dimensional structure analysis, respectively.

Appendix A. Supplementary data

Supplementary data to this article can be found online at https://doi.org/10.1016/j.ijbiomac.2025.142843.

References

[1] F. Bray, M. Laversanne, E. Weiderpass, I. Soerjomataram, The ever-increasing importance of cancer as a leading cause of premature death worldwide, Cancer 127 (2021), https://doi.org/10.1002/cncr.33587.
[2] J.M. Kocarnik, K. Compton, F.E. Dean, W. Fu, B.L. Gaw, J.D. Harvey, H. J. Henrikson, D. Lu, A. Pennini, R. Xu, E. Ababneh, et al., Cancer incidence, mortality, years of life lost, years lived with disability, and disability-adjusted life years for 29 Cancer groups from 2010 to 2019 a systematic analysis for the global burden of disease study 2019, JAMA Oncol. 8 (2022), https://doi.org/10.1001/jamaoncol.2021.6987.
[3] H. Patel, J. Li, L. Bo, R. Mehta, C.R. Ashby, S. Wang, W. Cai, Z.S. Chen, Nanotechnology-based delivery systems to overcome drug resistance in cancer, Med. Rev. 4 (2024), https://doi.org/10.1515/mr-2023-0058.
[4] M. Ebrahimnia, S. Alavi, H. Vaezi, M.K. Iradmousa, A. Haeri, Exploring the vast potentials and probable limitations of novel and nanostructured implantable drug delivery systems for cancer treatment, EXCLI J. 23 (2024), https://doi.org/10.17179/excli2023-6747.
[5] L. Miao, C.M. Lin, L. Huang, Stromal barriers and strategies for the delivery of nanomedicine to desmoplastic tumors, J. Control. Release 219 (2015) 192–204, https://doi.org/10.1016/j.jconrel.2015.08.017.
[6] S.M.P. Vadevoo, S. Gurung, H.S. Lee, G.R. Gunassekaran, S.M. Lee, J.W. Yoon, Y. K. Lee, B. Lee, Peptides as multifunctional players in cancer therapy, Exp. Mol. Med. 55 (2023), https://doi.org/10.1038/s12276-023-01016-x.
[7] N. Ghadiri, M. Javidan, S. Sheikhi, Ö. Taştan, A. Parodi, Z. Liao, M. Tayybi Azar, M. Ganjalıkhani-Hakemi, Bioactive peptides: an alternative therapeutic approach for cancer management, Front. Immunol. 15 (2024), https://doi.org/10.3389/fimmu.2024.1310443.
[8] X. Li, H. Zhong, S. Zheng, J. Mu, N. Yu, S. Guo, Tumor-penetrating iRGD facilitates penetration of poly(floxuridine-ketal)-based nanomedicine for enhanced pancreatic cancer therapy, J. Control. Release 369 (2024) 444–457, https://doi.org/10.1016/J.JCONREL.2024.04.004.
[9] R. Wei, J. Li, W. Lin, X. Pang, H. Yang, S. Lai, X. Wei, X. Jiang, Y. Yuan, R. Yang, Nanoparticle-mediated blockade of CXCL12/CXCR4 signaling enhances glioblastoma immunotherapy: monitoring early responses with MRI radiomics, Acta Biomater. 177 (2024), https://doi.org/10.1016/j.actbio.2024.02.007.
[10] S. He, Y. Fang, M. Wu, P. Zhang, F. Gao, H. Hu, C. Sheng, G. Dong, Enhanced tumor targeting and penetration of proteolysis-targeting chimeras through iRGD peptide conjugation: a strategy for precise protein degradation in breast Cancer, J. Med. Chem. 66 (2023), https://doi.org/10.1021/acs.jmedchem.3c01539.
[11] V.M. D'Amore, G. Donati, E. Lenci, B.S. Ludwig, S. Kossatz, M. Baiula, A. Trabocchi, H. Kessler, F.S. Di Leva, L. Marinelli, Molecular view on the iRGD peptide binding mechanism: implications for integrin activity and selectivity

profiles, J. Chem. Inf. Model. 63 (2023), https://doi.org/10.1021/acs.jcim.3c01071.
[12] S.J. Wang, S.K. Dougan, M. Dougan, Immune mechanisms of toxicity from checkpoint inhibitors, Trends in Cancer 9 (2023), https://doi.org/10.1016/j.trecan.2023.04.002.
[13] D. Yadav, M. Kwak, P.S. Chauhan, N. Puranik, P.C.W. Lee, J.O. Jin, Cancer immunotherapy by immune checkpoint blockade and its advanced application using bio-nanomaterials, Semin. Cancer Biol. 86 (2022), https://doi.org/10.1016/j.semcancer.2022.02.016.
[14] Q. Li, L. Quan, J. Lyu, Z. He, X. Wang, J. Meng, Z. Zhao, L. Zhu, X. Liu, H. Li, Discovery of peptide inhibitors targeting human programmed death 1 (PD-1) receptor, Oncotarget 7 (2016), https://doi.org/10.18632/oncotarget.11274.
[15] S. Gurung, F. Khan, G.R. Gunassekaran, J. Do Yoo, S.M. Poongkavithai Vadevoo, U. Permpoon, S.H. Kim, H.J. Kim, I.S. Kim, H. Han, J.H. Park, S. Kim, B. Lee, Phage display-identified PD-L1-binding peptides reinvigorate T-cell activity and inhibit tumor progression, Biomaterials 247 (2020), https://doi.org/10.1016/j.biomaterials.2020.119984.
[16] L. Wang, N. Wang, W. Zhang, X. Cheng, Z. Yan, G. Shao, X. Wang, R. Wang, C. Fu, Therapeutic peptides: current applications and future directions, Signal Transduct. Target. Ther. 7 (2022), https://doi.org/10.1038/s41392-022-00904-4.
[17] B. Zhang, S. Wan, X. Peng, M. Zhao, S. Li, Y. Pu, B. He, Human serum albumin-based doxorubicin prodrug nanoparticles with tumor pH-responsive aggregation-enhanced retention and reduced cardiotoxicity, J. Mater. Chem. B 8 (2020) 3939–3948, https://doi.org/10.1039/D0TB00327A.
[18] Q. Pan, X. Fan, L. Xie, D. Wu, R. Liu, W. Gao, K. Luo, B. He, Y. Pu, Nano-enabled colorectal cancer therapy, J. Control. Release 362 (2023) 548–564, https://doi.org/10.1016/J.JCONREL.2023.09.014.
[19] B. Godin, E. Tasciotti, X. Liu, R.E. Serda, M. Ferrari, Multistage Nanovectors: From Concept to Novel Imaging Contrast Agents and Therapeutics (2011), https://doi.org/10.1021/AR200077P.
[20] P. Sahandi Zangabad, M. Karimi, F. Mehdizadeh, H. Malekzad, A. Ghasemi, S. Bahrami, H. Zare, M. Moghoofei, A. Hekmatmanesh, M.R. Hamblin, Nanocaged platforms: modification, drug delivery and nanotoxicity, Opening synthetic cages to release the tiger, Nanoscale 9 (2017) 1356–1392, https://doi.org/10.1039/C6NR07315H.
[21] E. Falvo, V. Damiani, G. Conti, F. Boschi, K. Messana, P. Giacomini, M. Milella, V. De Laurenzi, V. Morea, G. Sala, G. Fracasso, P. Ceci, High activity and low toxicity of a novel CD71-targeting nanotherapeutic named The-0504 on preclinical models of several human aggressive tumors, J. Exp. Clin. Cancer Res. 40 (2021), https://doi.org/10.1186/s13046-021-01851-8.
[22] E. Falvo, A. Arcovito, G. Conti, G. Cipolla, M. Pitea, V. Morea, V. Damiani, G. Sala, G. Fracasso, P. Ceci, Engineered human Nanoferritin bearing the drug Genz-644282 for Cancer therapy, Pharmaceutics 12 (2020) 992, https://doi.org/10.3390/pharmaceutics12100992.
[23] V. Damiani, E. Falvo, G. Fracasso, L. Federici, M. Pitea, V. De Laurenzi, G. Sala, P. Ceci, Therapeutic efficacy of the novel stimuli-sensitive nano-ferritins containing doxorubicin in a head and neck cancer model, Int. J. Mol. Sci. 18 (2017), https://doi.org/10.3390/ijms18071555.
[24] G. Conti, M. Pitea, R. Ossanna, R. Opri, G. Tisci, E. Falvo, G. Innamorati, E. Ghanem, A. Sbarbati, P. Ceci, G. Fracasso, Mitoxantrone-loaded nanoferritin slows tumor growth and improves the overall survival rate in a subcutaneous pancreatic cancer mouse model, Biomedicines 9 (2021), https://doi.org/10.3390/biomedicines9111622.
[25] G. Fracasso, E. Falvo, G. Colotti, F. Fazi, T. Ingegnere, A. Amalfitano, G. B. Doglietto, S. Alfieri, A. Boffi, V. Morea, G. Conti, E. Tremante, P. Giacomini, A. Arcovito, P. Ceci, Selective delivery of doxorubicin by novel stimuli-sensitive nano-ferritins overcomes tumor refractivity, J. Control. Release (2016), https://doi.org/10.1016/j.jconrel.2016.08.010.
[26] F. Marrocco, E. Falvo, L. Mosca, G. Tisci, A. Arcovito, A. Reccagni, C. Limatola, R. Bernardini, P. Ceci, G. Colotti, ARTICLE Nose-to-brain selective drug delivery to glioma via ferritin-based nanovectors reduces tumor growth and improves survival rate, (n.d.). doi:https://doi.org/10.1038/s41419-024-06653-2.
[27] Z. Zhen, W. Tang, H. Chen, X. Lin, T. Todd, G. Wang, T. Cowger, X. Chen, J. Xie, RGD-modified Apoferritin nanoparticles for efficient drug delivery to tumors, ACS Nano 7 (2013) 4830–4837, https://doi.org/10.1021/nn305791q.
[28] C. Huang, C. Chu, X. Wang, H. Lin, J. Wang, Y. Zeng, W. Zhu, Y.-X.J. Wang, G. Liu, Ultra-high loading of sinoporphyrin sodium in ferritin for single-wave motivated photothermal and photodynamic co-therapy, Biomater. Sci. 5 (2017) 1512–1516, https://doi.org/10.1039/C7BM00302A.
[29] C. Wang, X. Wang, W. Zhang, D. Ma, F. Li, R. Jia, M. Shi, Y. Wang, G. Ma, W. Wei, Shielding ferritin with a biomineralized shell enables efficient modulation of tumor microenvironment and targeted delivery of diverse therapeutic agents, Adv. Mater. 34 (2022) 2107150, https://doi.org/10.1002/ADMA.202107150.
[30] Y. Lei, Y. Hamada, J. Li, L. Cong, N. Wang, Y. Li, W. Zheng, X. Jiang, Targeted tumor delivery and controlled release of neuronal drugs with ferritin nanoparticles to regulate pancreatic cancer progression, J. Control. Release 232 (2016) 131–142, https://doi.org/10.1016/j.jconrel.2016.03.023.
[31] N.K. Lee, E.J. Lee, S. Kim, G. Hoon Nam, M. Kih, Y. Hong, C. Jeong, Y. Yang, Y. Byun, I.S. Kim, Ferritin nanocage with intrinsically disordered proteins and affibody: a platform for tumor targeting with extended pharmacokinetics, J. Control. Release 267 (2017) 172–180, https://doi.org/10.1016/j.jconrel.2017.08.014.
[32] G. Deng, Y. Li, N. Liang, P. Hu, Y. Zhang, L. Qiao, Y. Zhang, J. Xie, H. Luo, F. Wang, F. Chen, F. Liu, D. Xu, J. Zhang, Ferritin in cancer therapy: a pleiotropic tumoraffin nanocage-based transport, Cancer Med. 12 (2023) 11570–11588, https://doi.org/10.1002/CAM4.5778.
[33] W. Yan, H. Li, J. Ning, S. Huang, L. Jiang, P. Xu, M. Huang, C. Yuan, Engineered protein cages with enhanced extracellular drug release for elevated antitumor efficacy, Int. J. Biol. Macromol. 267 (2024) 131492, https://doi.org/10.1016/J.IJBIOMAC.2024.131492.
[34] J. He, K. Fan, X. Yan, Ferritin drug carrier (FDC) for tumor targeting therapy, J. Control. Release 311–312 (2019) 288–300, https://doi.org/10.1016/j.jconrel.2019.09.002.
[35] Q. Liu, C. Wang, M. Zhu, J. Liu, Q. Duan, A.C. Midgley, R. Liu, B. Jiang, D. Kong, Q. Chen, J. Zhuang, X. Huang, Self-assembly of heterogeneous ferritin Nanocages for tumor uptake and penetration, Adv. Sci. 11 (2024), https://doi.org/10.1002/advs.202309271.
[36] E. Falvo, F. Malagrinò, A. Arcovito, F. Fazi, G. Colotti, E. Tremante, P. Di Micco, A. Braca, R. Opri, A. Giuffrè, G. Fracasso, P. Ceci, The presence of glutamate residues on the PAS sequence of the stimuli-sensitive nano-ferritin improves in vivo biodistribution and mitoxantrone encapsulation homogeneity, J. Control. Release 275 (2018) 177–185, https://doi.org/10.1016/J.JCONREL.2018.02.025.
[37] G. Fracasso, E. Falvo, G. Tisci, G. Sala, G. Colotti, S. Cingarlini, C. Tito, S. Bibbo, C. Frusteri, E. Tremante, E. Giordani, P. Giacomini, P. Ceci, Widespread in vivo efficacy of The-0504: a conditionally-activatable nanoferritin for tumor-agnostic targeting of CD71-expressing cancers, Heliyon 9 (2023), https://doi.org/10.1016/j.heliyon.2023.e20770.
[38] S. Modi, W. Jacot, T. Yamashita, J. Sohn, M. Vidal, E. Tokunaga, J. Tsurutani, N. T. Ueno, A. Prat, Y.S. Chae, K.S. Lee, N. Niikura, Y.H. Park, B. Xu, X. Wang, M. Gil-Gil, W. Li, J.-Y. Pierga, S.-A. Im, H.C.F. Moore, H.S. Rugo, R. Yerushalmi, F. Zagouri, A. Gombos, S.-B. Kim, Q. Liu, T. Luo, C. Saura, P. Schmid, T. Sun, D. Gambhire, L. Yung, Y. Wang, J. Singh, P. Vitazka, G. Meinhardt, N. Harbeck, D. A. Cameron, Trastuzumab Deruxtecan in previously treated HER2-low advanced breast Cancer, N. Engl. J. Med. 387 (2022) 9–20, https://doi.org/10.1056/nejmoa2203690.
[39] I.S. Jeon, J. Do Yoo, S. Gurung, M. Kim, C. Lee, E.J. Park, R.W. Park, B. Lee, S. Kim, Anticancer nanocage platforms for combined immunotherapy designed to harness immune checkpoints and deliver anticancer drugs, Biomaterials 270 (2021), https://doi.org/10.1016/j.biomaterials.2021.120685.
[40] H.B. Pang, G.B. Braun, Z.G. She, V.R. Kotamraju, K.N. Sugahara, T. Teesalu, E. Ruoslahti, A free cysteine prolongs the half-life of a homing peptide and improves its tumor-penetrating activity, J. Control. Release 175 (2014), https://doi.org/10.1016/j.jconrel.2013.12.006.
[41] J.M. Seligson, A.M. Patron, M.J. Berger, R.D. Harvey, N.D. Seligson, Sacituzumab Govitecan-hziy: an antibody-drug conjugate for the treatment of refractory, metastatic, triple-negative breast Cancer, Ann. Pharmacother. 55 (2021), https://doi.org/10.1177/1060028020966548.
[42] T.M. Cardillo, S.V. Govindan, R.M. Sharkey, P. Trisal, R. Arrojo, D. Liu, E.A. Rossi, C.H. Chang, D.M. Goldenberg, Sacituzumab govitecan (IMMU-132), an Anti-Trop-2/SN-38 antibody-drug conjugate: characterization and efficacy in pancreatic, gastric, and other cancers, Bioconjug. Chem. 26 (2015), https://doi.org/10.1021/acs.bioconjchem.5b00223.